Environmental Reconstruction of Anoxic Marine Systems: Core Black Shales of Upper Pennsylvanian Midcontinent Cyclothems

Thomas J. Algeo[1], David L. Hoffman[1,*],
J. Barry Maynard[1], Michael M. Joachimski[2],
James C. Hower[3,4], and W. Lynn Watney[5,6]

[1] H. N. Fisk Laboratory of Sedimentology
Department of Geology
University of Cincinnati
Cincinnati, OH 45221-0013

[*] Present address:
Burns & McDonnell
165 EAB Plaza, 6W
Uniondale, NY 11556-0165

[2] Institut für Geologie
Schlossgarten 5
University of Erlangen-Nürnberg
91054 Erlangen, Germany

[3] Center for Applied Energy Research
3572 Iron Works Pike
Lexington, KY 40511-8433

[4] Department of Geological Sciences
University of Kentucky
Lexington, KY 40506-0059

[5] Kansas Geological Survey
1930 Constant Avenue
Lawrence, KS 66047-3724

(In: Algeo, T.J., and Maynard, J.B. (Eds.), 1997. *Cyclic Sedimentation of Appalachian Devonian and Midcontinent Pennsylvanian Black Shales: Analysis of Ancient Anoxic Marine Systems—A Combined Core and Field Workshop*: Joint Meeting of Eastern Section AAPG and The Society for Organic Petrography (TSOP), Lexington, Kentucky, Sept. 27-28, 1997, p. 103-147.)

ABSTRACT

Environmental analysis of offshore shale members of Upper Pennsylvanian Midcontinent cyclothems was undertaken using a combination of high-resolution X-radiography, petrography, and geochemical analyses. A hierarchical sampling strategy permitted investigation of (1) broad stratigraphic and geographic patterns of compositional variation through analysis of three shale members (Hushpuckney, Stark, and Muncie Creek) in five cores along a proximality gradient, and (2) fine stratigraphic variation within each study unit through continuous cm-scale sampling of dm-thick compositional cycles. Offshore shales consist of (1) three major non-clastic components, i.e., organic carbon, Fe-sulfide, and phosphate, which can be effectively proxied by TC, TS, and P_2O_5, respectively, and (2) a clay-mineral matrix composed predominantly of illite and smectite (or mixed-layer I/S), the relative proportions of which can be proxied by Al_2O_3/SiO_2 ratios. Spatio-temporal variation in sediment fluxes permitted identification of two clastic components: (1) a southern-derived smectite-rich component associated with high concentrations of inertinite, and (2) a northern-derived illite-rich component associated with high concentrations of vitrinite. Strong covariation between the flux of the illitic component and TOC concentrations implies control of sediment composition by an *organic* dilution process associated with variable influx of low-salinity surfacewaters from continental areas to the north or northeast. Cm-scale correlation within each offshore shale member across the 150-200-km-long study area based on (1) alternating dm-thick high-TOC and low-TOC layers and (2) systematic upsection changes in phosphate layer character (from thin laminae to large nodules to diaclasts and wispy laminae) demonstrated an absence of intraformational erosion and winnowing, suggesting widely uniform sub-pycnocline conditions and a lack of strong bottom currents. Authigenic phosphate (1) is concentrated at a fine scale along the upper and lower contacts of high-TOC layers, and (2) mirrors broad spatio-temporal patterns of variation in bottomwater anoxia; these observations suggest control of phosphate formation by a combination of slow sedimentation rates, permitting downward diffusion of seawater PO_4^{3-} and slow nodule growth, and low but fluctuating bottomwater oxygen levels (e.g., ca. 0.1-0.2 ml O_2 l^{-1} H_2O), permitting retention of PO_4^{3-} through redox cycling of iron oxyhydroxides. These observations favor a model for the Late Pennsylvanian Midcontinent Seaway of starved sedimentation under a strong proximal halocline that was subject to fluctuations at timescales associated with the deposition of dm-thick compositional cycles; upwelling intensity was weak and evidence for upwelling-enhanced primary productivity is lacking.

INTRODUCTION

The environmental conditions under which organic matter accumulates in abundance can be quite variable. A feature common to most models for organic-rich facies is enhanced preservation of organic matter as a result of water-column stratification and development of bottomwater anoxia (e.g., Demaison and Moore 1980; Arthur and Sageman 1994). Other environmental factors within anoxic systems typically are more difficult to evaluate, e.g., stratification type, primary productivity, clastic dilution, terrigenous organic flux, and benthic sediment irrigation, as well as the interplay of these parameters with bottomwater oxygen levels, although such factors are crucial to an understanding of controls on organic matter accumulation in modern anoxic marine environments (e.g., Ittekkot et al. 1992; Shimmield 1992; Martens 1993; Lyons et al. 1993; Canfield 1994; Calvert et al. 1996). In this paper, we will address relationships among most of these parameters within offshore black shales of Upper Pennsylvanian cyclothems from Midcontinent North America, including (1) the effect of pycnocline strength on organic matter accumulation, (2) relative fluxes of terrigenous-derived clastics and organic matter, and operation of clastic vs. organic dilution processes, (3) multiple sediment fluxes to the depositional environment, and their relation to bottomwater oxygen levels, and (4) relations of degree-of-anoxia indices to benthic activity levels and organic matter concentrations. Detailed environmental analyses of this type for individual ancient anoxic marine systems have the potential to provide new insights on controls on organic matter accumulation and to permit refinement of existing environmental models for organic-rich facies.

Analysis of environmental conditions within anoxic marine systems is hampered in part by the compositional complexity of organic-rich sediments, to which a large number of analytical techniques must be applied in order to characterize such basic parameters as bulk sediment geochemistry, type and condition of organic matter, mineralogy and grain size of the detrital fraction, distribution of authigenic components, stratification patterns, ichnofabrics, and fossil content (e.g., Stein 1991). Although many studies utilize a limited number of geochemical techniques, a thorough understanding of controls on organic matter accumulation requires a comprehensive analysis of compositional variation. Further, because different processes may operate with differing intensities at various temporal and geographic scales, it is desirable to analyze variation in environmental parameters (1) at a fine scale (e.g., mm-thick laminae), in order to minimize interference among multiple depositional processes (e.g., Hay et al. 1990; Aplin et al. 1992; Martens 1993), and (2) at a coarse scale, in order to investigate broad regional and secular changes in environmental conditions (e.g., Burnett 1980; Mossmann et al. 1991). Whereas analysis of fine-scale compositional variation in organic-rich sediments over long stratigraphic intervals is impractical using standard techniques, a new procedure combining high-resolution X-radiography of black shale cores with petrographic and geochemical analyses of limited core intervals using a hierarchical sampling strategy permits efficient characterization of mm-scale compositional variation over stratigraphic intervals of meters to tens of meters (Hoffman et al. 1997; Jaminski et al. 1997; Algeo et al., companion paper). In this paper, we will report on an integrated multi-technique analysis of Upper Pennsylvanian offshore shales in Midcontinent North America with the goals of (1) applying X-radiography in delineation of mm-scale patterns of compositional variation within eight study units averaging 50 cm in thickness, (2) establishing a correlatable, high-resolution (cm-scale) internal stratigraphic framework for each offshore shale to facilitate analysis of regional variation in environmental parameters, and (3) reconstructing environmental conditions and processes during deposition of offshore shales within the Midcontinent Seaway.

PALEOGEOGRAPHIC AND PALEOCLIMATIC SETTING

Upper Pennsylvanian strata of Midcontinent North America are exposed in a 500-km-long belt extending from Oklahoma in the south to Iowa and Nebraska in the north. The five cores of the present study are located in eastern Kansas, within the central part of this outcrop belt, and span a distance of ca. 200 km (Fig. 1). The study cores provide a paleoenvironmental transect across the Eastern Midcontinent Shelf with more proximal settings to the north and more distal settings to the south. The southern margin of the shelf was approximately coincident with the boundary between the phylloid algal mound and terrigenous detrital facies belts in southeastern Kansas (Heckel 1977). From a paleotectonic perspective, the Eastern Midcontinent Shelf was separated from the active Ouachita-Marathon and Ozark uplifts to the south and southeast by the narrow but intermittently deep Anadarko and Arkoma foreland basins (Fig. 2; Arbenz 1989). A low-lying cratonic landmass was present to the north, but low topographic relief on the Midcontinent Shelf resulted in lateral shifts in the paleo-shoreline over distances of hundreds of kilometers in response to sea-level fluctuations (Heckel 1986; Boardman and Heckel 1989).

The study area in eastern Kansas was located at 5-10°N latitude during the Late Pennsylvanian (Fig. 2; Heckel 1977; Scotese 1994). General atmospheric circulation climate models (GCMs) suggest that Midcontinent North America had a temperate climate (10-25°C), limited seasonal temperature range (<15°C), and moderate annual precipitation (<73 cm yr^{-1}) at that time (Crowley et al. 1989; Crowley et al. 1996). These conditions are consistent with development of vertisols and aridosols in the Midcontinent during the Late Pennsylvanian, the modern counterparts of which form under strongly seasonal climates with precipitation of 25-100 cm yr^{-1} (Schutter and Heckel 1985). The peri-equatorial position of the Appalachian-Hercynian orogenic belt may have enhanced zonal atmospheric circulation (Fig. 2), although monsoonal circulation may have existed owing to (1) a large interhemispheric thermal contrast, and (2) a source of moisture and latent energy in the large

Tethyan oceanic embayment to the east (Parrish 1993; Crowley et al. 1996). These factors would have contributed not only to seasonal but also to long-period climatic cyclicity through modulation of seasonality and monsoonal intensity by, e.g., orbital forcing (Parrish 1993; Crowley et al. 1996).

MISSOURIAN STAGE STRATIGRAPHY

The Missourian Stage (lower Upper Pennsylvanian) of Midcontinent North America comprises 3 groups (Pleasanton, Kansas City, and Lansing, in ascending stratigraphic order), 12 formations, and about 38 members (Fig. 3; Watney et al. 1989). In this area, the Missourian succession consists mainly of interstratified marine shales and limestones deposited in 10-50-m-thick transgressive-regressive sequences known as cyclothems. Upper Pennsylvanian cyclothems were produced by quasi-periodic global sea-level fluctuations resulting from waxing and waning of continental icesheets during the Gondwanan Ice Age (Crowell 1978; Veevers and Powell 1987; Heckel 1994). Kansas-type cyclothems (as opposed to coal-bearing cyclothems of the Illinois Basin) are predominantly composed of marine limestones and shales and commonly exhibit a succession of four members (in ascending stratigraphic order): (1) a middle or transgressive limestone, (2) a core or offshore shale, (3) an upper or regressive limestone, and (4) an outside or nearshore shale (Heckel 1977). For the most part, formations are equivalent to cyclothems (which are named for the regressive limestone, usually the thickest member), resulting in stratigraphic assignment of core black shales as members of formations.

In a sequence stratigraphic context, offshore shales represent condensed horizons associated with maximum flooding surfaces (Watney et al. 1995). Many of these organic-rich shales are laterally continuous over distances of >600 km along an outcrop belt from western Iowa to northeastern Oklahoma and persist in the subsurface several hundred kilometers further south into north-central Texas (Wanless and Wright 1978; Heckel 1986, 1991; Boardman and Heckel 1989). Subsurface gamma-ray studies have extended these correlations over 650 km westward into western Kansas and eastern Colorado, demonstrating the broad areal continuity of offshore shales in Upper Pennsylvanian cyclothems (Watney 1980; Watney et al. 1995).

In this study, three offshore shales from the Kansas City Group were examined: (1) the Hushpuckney Member of the Swope Formation, (2) the Stark Member of the Dennis Formation, and (3) the Muncie Creek Member of the Iola Formation (Fig. 3). In the study cores, these shales consist of a 50(±10)-cm-thick, laminated, non-fossiliferous, black, organic-rich facies overlain by a 20(±10)-cm-thick, bioturbated, sparsely fossiliferous, gray, organic-poor facies (n.b., this study focuses exclusively on the organic-rich facies). Contacts with subjacent transgressive limestones are sharp, although the underlying carbonates commonly contain shale-filled burrows and the contact itself may comprise a carbonate skeletal clast lag. The organic-rich facies of offshore shales commonly exhibit alternating dark gray (Munsell 10 YR 6/1-5/1), organic-"poor" (10-20 wt% TOC) and black (Munsell 10 YR 3/1-2/1), organic-rich (20-40 wt% TOC) layers. These couplets, which range from about 5 to 15 cm in thickness, are weakly visible on the surfaces of study cores but are strongly enhanced in X-radiographs. Disseminated Fe-sulfides and laminar or nodular phosphatic layers of authigenic origin are present throughout the study cores.

METHODS

Analytical Strategy

Fine-scale compositional variation in laminated organic-rich shales can be studied effectively through a combination of X-radiographic, petrographic, and geochemical techniques (Hoffman et al. 1997; Jaminski et al. 1997; Algeo et al., companion paper). Whole-core X-radiography allows imaging of compositionally-based variation in rock density at a sub-millimeter scale, and geochemical and petrographic analysis of selected stratigraphic intervals permits identification of compositional controls on rock-density variation at a centimeter-scale. X-radiographic analysis of compositional variation in organic-rich shales is facilitated by (1) differences in density between the major non-clastic components of the shale (i.e., organic carbon, Fe-sulfide, and phosphate) and its clay-mineral matrix, and (2) availability of reliable elemental proxies for the major components.

Environmental parameters may exhibit strong spatial and temporal dependence, i.e., different conditions and processes may operate over short vs. long distances and at low vs. high frequencies. A thorough understanding of environmental conditions thus requires analysis of compositional variation at multiple length scales in both the lateral and stratigraphic dimensions. In this study, a hierarchical sampling strategy was adopted to allow investigation of patterns of compositional variation in four "dimensions": (1) interformational variation, i.e., between several offshore shales, (2) lateral variation, i.e., along a proximality gradient within a single offshore shale, (3) intraformational variation, i.e., over the entire stratigraphic range (base to top) of each study unit, and (4) intracyclic variation, i.e., at a centimeter scale within dm-thick compositional cycles (Fig. 4).

A total of eight study units, drawn from three stratigraphic horizons (Hushpuckney, Stark, and Muncie Creek shales) and five cores (Edmonds, Ermal, Womelsdorf, Mitchellson, and Heilman), were examined (Fig. 4). The Hushpuckney and Stark shales were examined in three and four of the five study cores, representing north-south transects of ca. 150 km and ca. 200 km, respectively, along the Eastern Midcontinent Shelf (Fig. 1). With regard to proximality trends, northern locales (e.g., Edmonds) are proximal and southern locales (e.g., Heilman) are distal. Not every shale member was examined in each of the five study cores; in particular, the Muncie Creek Shale was examined in a single core mainly in order to compare environmental parameters of lower Missourian Stage shales (i.e., Hushpuckney and Stark) with those of an upper Missourian Stage shale (i.e., Muncie Creek).

X-Radiography & Sampling Procedure

X-radiography served as a primary analytical tool for (1) identification of patterns of fine-scale compositional variation in the study cores, permitting optimization of sample locations, (2) generation of high-resolution gray-scale density (GSD) records that served as a proxy rock-density record and that allowed GSD-elemental correlation, and (3) visual inspection of the distribution of certain authigenic components (e.g., phosphate; Fig. 5). For a sample of uniform thickness, contrast in X-radiograph images is due to compositionally-based differences in rock density such that denser (less dense) areas appear lighter (darker) owing to reduced (increased) X-ray penetration (e.g., Algeo and Woods 1994; Algeo et al. 1994; Jaminski et al. 1997). X-radiographic analysis of compositional variation in the study units depended on differences in density between the major non-clastic components of the shale (e.g., organic carbon, Fe-sulfide, and phosphate, with densities of 1.0-1.2, 5.1-5.2, and 3.1-3.2 g cm^{-3}, respectively) and its clay-mineral matrix (2.6-2.7 g cm^{-3}), which is composed largely of illite, smectite, and mixed-layer illite/smectite. X-radiograph images were produced at the University of Cincinnati using a tungsten-source Hewlett Packard Faxitron (model 43804N) and a custom-built core stage consisting of a platform driven by a variable-speed step motor. Details of X-radiographic methods and procedures for estimation of elemental concentrations from X-radiograph GSD values are given in Algeo et al. (companion paper).

The sampling protocol for each study unit entailed collection of samples of sub-equal thickness (0.6-2.0 cm; mean 1.2 cm) (1) discontiguously, at 5-10 cm intervals, from the base to the top of the unit to characterize intraformational variation, and (2) contiguously over a 12-16-cm thick stratigraphic interval corresponding to at least one complete compositional cycle to characterize intracyclic variation (Fig. 4). Compositional cycles for detailed analysis were chosen from the mid-lower half of each study unit; approximately correlative horizons were selected within each shale member to facilitate analysis of lateral trends (Fig. 5). Within cycles, sample boundaries were located on the basis of core X-radiographs to coincide with natural compositional breaks. Samples were ground in an agate ball mill and stored in nitrogen-filled vials and refrigerated to prevent oxidation of organic carbon and sulfides prior to analysis. A total of 85 samples were collected from the eight study units.

Mineralogic and Petrographic Analysis

X-ray diffraction (XRD) analysis was undertaken on randomly oriented pressed-powder mounts for whole-rock and clay-mineral samples. Clay-mineral separates were prepared by dispersing powdered samples in deionized water using 0.02 N sodium pyrophosphate, repeatedly resuspending the sample until particles remained in suspension for at least 12 hours, centrifuging the suspension, and resuspending the centrifuged residue for transfer to sample mounts. Glycolated samples were prepared using ethylene glycol and heated at 60°C for 24 hours. Sample mounts were analyzed with a fully-automated Siemens D-500 X-ray diffractometer at the University of Cincinnati, using copper K_α radiation and a monochromator. Samples were scanned at a rate of $0.2° s^{-1}$ over the 2Θ range of 2° to 70° for whole-rock samples and 2° to 32° for clay-mineral separates. Clay minerals were identified by basal peaks (00l) on diffractograms, and semi-quantitative analysis of clay-mineral abundances followed methods outlined by Johns et al. (1954) and Biscaye (1965).

Petrographic components were examined in polished slabs under both reflected white and violet-UV fluorescent light (Robl et al. 1991), and organic macerals were classified using a standard nomenclature (Hutton 1987; Tyson 1995). Point-counting was used to determine the relative frequencies of different petrographic components, and observations were made using a 0.3x0.3 mm grid. For each sample zone, a minimum of 300 observations were collected such that all linear traverses perpendicular to bedding were completed. Point-counts were undertaken on 56 sample zones.

Carbon-Sulfur Elemental Analysis

Carbon and sulfur elemental concentrations were measured on a whole-rock basis, yielding total carbon (TC) and total sulfur (TS) values in weight percent, using a LECO CS-244 analyzer at the Kentucky Geological Survey. A laboratory standard was run before and after each set of fifteen samples to monitor instrument drift. Analytical precision (2σ) was ±2.0% for TC and ±7.6% for TS of measured concentrations based on 15 replicate analyses. A total of 106 samples were analyzed, i.e., the 85 samples from the eight core intervals chosen for detailed study (see sampling procedure above) plus another 21 samples from the base and top of the Stark Shale at several locales; the latter set was intended to document stratigraphic variation in TC and TS content within this formation. A representative subset of samples ($n = 17$), including material from each study formation and locale, was analysed for inorganic C content using a carbonate bomb. These samples yielded uniformly low values ($\mu \pm \sigma = 1.2 \pm 0.9\%$ of total carbon) with an analytical uncertainty of ±16%(2σ) of reported values owing to extrapolation of the regression line for $CaCO_3$ standards. In view of the small fractional contribution of inorganic carbon to total carbon, it was deemed unnecessary to determine the inorganic C content of the full sample set.

Organic Carbon Isotopic Analysis

About two-thirds of the sample set ($n = 61$) was analyzed for bulk organic carbon $\delta^{13}C$. Samples were treated with hot concentrated HCl to remove carbonates and then washed with deionized water to neutrality. Samples were combusted with CuO at 850°C in quartz tubes, and the evolved CO_2 was purified by cryogenic distillation. Isotopic analyses were performed at the University of Erlangen-Nürnberg using a Finnegan MAT 252 mass spectrometer. Reproducibility was checked by repeated measurements of graphite standard USGS 24 and is better than ±0.1 ‰.

Major- and Trace-Element Analysis

About 4-5 g of each sample were pressed into a pellet and analyzed for whole-rock elemental concentrations using a wavelength-dispersive Rigaku 3040 XRF spectrometer at the University of Cincinnati. Analysis included one run for major elements (including S, P, Ca, and Fe) and one for trace elements. XRF intensities were calibrated using both USGS (SDO-1, SCo-1, SGR-1) and internal black shale standards (analyzed using XRF and INAA by XRAL Incorporated). Analytical precision based on replicate analyses was better than ±1% for Zr, Y, and Rb, ±3.2% for Mn, ±3.8% for Na, ±5% for other trace elements, and ±2% for other major and minor elements. Detection limits for trace elements were 5 ppm for Nb, Zr, Y, Sr, Rb, Zn, Cu, and Ni, 15 ppm for Cr and V, 20 ppm for U, and 50 ppm for Ba. Leco- and XRF-determined S values were in good agreement ($m = 1.00$, $r^2 = 0.82$). See Hoffman et al. (1997) for presentation of trace-element concentration data.

RESULTS

Elemental Proxies for Major Components

The major non-clastic components of the study units were determined by petrographic and geochemical methods to be organic matter, Fe-sulfide (mainly pyrite), and phosphate (Fig. 6). These components can be effectively proxied by total carbon (TC), total sulfur (TS), and P_2O_5, respectively: (1) organic carbon represents, on average, 99.1±0.9% of TC (Algeo et al., companion paper), (2) the weight fraction of sulfide sulfur in TS is uncertain but likely to be ca. 60-90% (cf. Kaplan et al. 1963; Mossmann et al. 1991; Chu et al. 1993; Schimmelmann and Kastner 1993), and (3) strong P_2O_5-CaO covariation ($r^2 = 0.95$) and a bimodal distribution of P_2O_5 values (i.e., a mode at <0.5 wt% associated with samples lacking nodules and a mode at >5.0 wt% associated with those containing nodules) suggests that phosphorus is concentrated mainly (i.e., >90%) in authigenic phosphate nodules (Algeo et al., companion paper).

The detrital component of the study units consists of several minerals. Whole-rock XRD analysis determined that the detrital component is clay-mineral dominated, and diffractograms of clay-mineral separates identified the dominant clay minerals as smectite (or mixed-layer illite/smectite, I/S) and illite, with minor quantities of chlorite and kaolinite. Because variation in the relative abundances of different clay minerals is of greater environmental significance than variation in the weight fraction of the detrital component (which covaries inversely with Corg content owing to a dilution relationship), elemental proxies were developed for the dominant clay minerals using XRF data. Strong negative covariance of SiO_2* with all other detrital elements (i.e., Al_2O_3*, Fe_2O_3*, K_2O*, MgO*, TiO_2*, and Na_2O*) is consistent with a predominantly two-phase detrital component (Table 1; asterisks indicate normalization on a C-, S-, and P-free basis). Given a paucity of quartz (verified by XRD and petrographic analysis of the study units), Al_2O_3*/SiO_2* ratios are a useful proxy for clay mineralogy, e.g., 0.25-0.36 for smectite, 0.38-0.56 for illite, 0.64-0.85 for kaolinite, and 0.70-1.0 for chlorite (Grim 1968; Weaver 1989). Comparison of these values with ratios observed in the study units, i.e., 0.29-0.74 with a strong primary mode at 0.32-0.42 (Fig. 7), suggests dominance of smectite or mixed-layer illite/smectite (I/S) with admixture of illite, kaolinite, or chlorite. Strong positive covariation of Al_2O_3*/SiO_2* ratios with K_2O* ($r^2 = 0.80$; Fig. 7A) and TiO_2* ($r^2 = 0.86$; Fig. 7B) implies mixing of two major clay-mineral phases and indicates that neither chlorite nor kaolinite (which are K- and Ti-poor) are present in significant quantities in samples with high Al_2O_3*/SiO_2* ratios. Hence, the major clay-mineral phases are likely to be a K- and Ti-poor smectite (or I/S) and a K- and Ti-rich illite.

X-radiographic Analysis of Compositional Variation

High-resolution X-radiographs of the study cores permitted detailed observations regarding compositional layering, ichnofabrics, and the distribution of authigenic precipitates (Fig. 5). Compositional layering is present throughout the laminated black shale facies of all study units at two distinct scales: (1) as faint, horizontal, sub-mm-thick laminae, and (2) as cm- to dm-thick bands of alternately dark and light layers. Evidence of bioturbation within the study units is limited to (1) isolated, 3- to 4-mm-diam. *Planolites* burrows in the Edmonds Muncie Creek (at 25-31 cm), and (2) networks of 0.5- to 1-mm-diam. *Trichichnus* and *Zoophycos* burrows within the black shale-gray shale transition of most study units (e.g., at 29-40 cm in the Ermal Hushpuckney and Mitchellson Hushpuckney; n.b., all locations of core features are relative to the base of the black shale facies, shown on vertical scale in Fig. 5). The distribution of Fe-sulfide is impossible to ascertain visually owing to its fine dissemination through the shale matrix, but the distribution of phosphate is easily determined owing its high density and distinctive morphology. Authigenic phosphate is found preferentially at the contacts of light and dark layers and, hence, appears to exhibit a genetic relationship to compositional banding. Although present in all shale members, phosphate nodules vary in abundance from low values in the Muncie Creek Shale to high values in the Hushpuckney Shale (Fig. 5).

Compositional variation within the study units can be quantified based on (1) differences in density between the major non-clastic components (i.e., organic carbon, Fe-sulfide, and phosphate) and the clay-mineral matrix, and (2) significant correlations between X-radiograph GSD (a proxy for rock density) and concentrations of elemental proxies for the major non-clastic components (Algeo et al., companion paper). Multiple regression of GSD on TC, TS, and P_2O_5 revealed that the three major non-clastic components collectively accounted for the majority of GSD variance in each shale member (71% in Hushpuckney, 87% in Stark, and 92% in Muncie Creek), providing a basis for compositional analysis using GSD values. Separate linear regressions of TC, TS, and P_2O_5 on GSD yielded significant correlations ($p(\alpha) < .05$) for (1) TC-GSD in seven of eight study cores (all except Mitchellson Hushpuckney; $r = -0.61$ to -0.97), (2) TS-GSD in one core (Heilman Stark; $r = +0.61$), and (3) P_2O_5-GSD in one core (Mitchellson Hushpuckney; $r = +0.87$). Based on these correlations, concentrations of elemental proxies for one or more of the major non-clastic components can be reliably estimated from GSD values in all study units (Algeo et al., companion paper). Concentration estimates based on GSD-elemental correlations allow construction of high-resolution (sub-cm-scale) geochemical proxy records over the full stratigraphic range of each study unit (Fig. 5; for consistency, all geochemical proxy columns are coded for TC variation; the distribution of phosphate, even in the Mitchellson Hushpuckney, is most reliably determined by visual inspection of core X-radiographs).

Compositional variation in the study cores at a centimeter-to-decimeter scale is primarily due to variation in organic carbon content, i.e., alternation of Corg-rich and Corg-poor layers. Corg-rich layers are present at 5-6, 9-10, 13-17, 19-23, and 28-31 cm in the Hushpuckney Shale (Fig. 5A), at 3-4, 6-7, 12-17, 20-22, 24-26, and 28-38 cm in the Stark Shale (Fig. 5B), and at 4-5, 7.5-8.5, 15.5-16.5, 18-19, 25-28, and 30-35 cm in the Muncie Creek Shale (Fig. 5A; n.b., depths are referenced to the Edmonds core). The thickness of high-Corg hemicycles increases progressively upsection in many units (e.g., Edmonds Stark), although Corg-rich intervals thicken to mid-section and then thin toward the top of some units (e.g., Womelsdorf Stark; Fig. 5B). Sub-cm-scale variation in organic carbon content exists in some study units, especially within Corg-rich layers (e.g., at 12-16 cm in Edmonds Stark; Fig. 5B), although the amplitude of such variation is generally smaller than that of cm- to dm-scale compositional cycles.

Much of the fine- (sub-cm-) scale compositional variation in the study cores is due to variable phosphate abundance. Authigenic phosphate nodules are easily recognized in core X-radiographs owing to their high density (i.e., dark color in X-radiograph prints such as Fig. 5) and distinctive morphology (i.e., large ovoid nodules, small in-situ diaclasts, and wispy irregular laminae). Individual phosphatic layers are thin (<1 cm, and commonly <1 mm) and tend to be laterally discontinuous at a centimeter scale. For the most part, phosphate layers occur in sets that are several centimeters in thickness; nodule character tends to be similar within each set but to differ between sets. In most study units, the character of phosphate nodules exhibits systematic stratigraphic variation. For example, in the Hushpuckney Shale, the sequence of morphologic types is (1) multiple, thin, laterally continuous laminae (e.g., at 1-3 and 10-11 cm), (2) rare, large, ovoid nodules (e.g., at 15-17 and 18-19 cm), and (3) multiple diaclasts and irregular, wispy laminae (e.g., at 20-22 and 26-28 cm; Fig. 5A). The same sequence is apparent in the Stark Shale, i.e., (1) thin continuous laminae at 1-2 cm, (2) large ovoid nodules at 11-14 cm (Ermal core only), and (3) diaclasts and wispy laminae at 27.5-28.5 cm (Fig. 5B), although stratigraphic variation in nodule type is somewhat less regular than in the Hushpuckney Shale.

Authigenic phosphate exhibits a pronounced association with Corg-rich core intervals. At a fine (i.e., cm) scale, phosphatic layers are preferentially concentrated at or near the upper and lower contacts of organic-rich layers (e.g., at 17-20 and 25-29 cm in Edmonds Stark; Fig. 5B). At a coarse (i.e., dm) scale, phosphate is more-or-less uniformly distributed within individual study units, although nodule abundance increases slightly upsection in the Stark Shale (i.e., Edmonds, Ermal, and Womelsdorf cores; Fig. 5B). These patterns of phosphate distribution differ somewhat from published observations for Midcontinent Pennsylvanian black shales. Kidder (1985) reported that the largest nodules and greatest nodule concentrations tended to be found at the top and bottom of black shale units. In the present study, the largest nodules are found in mid-unit (e.g., large, ovoid nodules at 10-30 cm in the Hushpuckney and Stark shales; Fig. 5), and the vertical distribution of phosphate is fairly uniform. Kidder (1985) and Ece (1987) reported geographic variation in phosphate morphology, i.e., nodular phosphate to the southwest and laminar phosphate to the northeast (n.b., study area ca. 20% larger than that of present study). In the present study, a weak trend of this type is apparent in mid-unit (e.g., Fig. 5B), but the most pronounced pattern is stratigraphic variation in nodule type from the base to the top of individual study units (see above).

X-radiographic Correlation of Study Units

Construction of multiple high-resolution geochemical proxy records for the Hushpuckney and Stark shales (e.g., Fig. 5) offers the potential for detailed internal stratigraphic correlation on a regional scale. Fine- (i.e., cm-) scale correlations are based on a hierarchy of features that are assigned either primary or secondary significance. The primary feature used in correlation is dm-scale cyclicity in the GSD record of each unit, which is mainly a reflection of variation in Corg content; these correlations are facilitated by systematic stratigraphic variation in the thickness of high-Corg hemicycles. Secondary correlation features include (1) characteristic patterns of cm-scale variation in GSD values (e.g., fine-scale cyclicity at 2-8 cm in Edmonds Stark; Fig. 5B), and (2) the presence and character of phosphate nodule sets. Cm- to dm-thick compositional layers are readily correlatable within each shale member across the full study area (i.e., 150 km for the Hushpuckney Shale, 200 km for the Stark Shale; Fig. 1).

The thickness of the laminated black shale facies of each shale member varies laterally in a fairly regular manner: (1) in the Hushpuckney Shale, from 40 cm (Mitchellson) to 60 cm (Edmonds; n.b., only lower 70% of Edmonds shown in Fig. 5A), and (2) in the Stark Shale, from 50 cm (Heilman) to 60 cm (Ermal and Edmonds; n.b., only lower 70-80% of each unit shown in Fig. 5B). Because the correlatable lower portions of each shale member are of nearly uniform thickness across the study area, thickness variation is largely confined to the upper 25-50% of each study unit, which also varies compositionally more than the lower portion of the black shale facies. Lateral compositional variation is not a function of geographic distance between study units, e.g., the thick Corg-rich layer at 30-38 cm in the Edmonds and Ermal Stark cores (139 km apart) is nearly absent 11 km further south in the Womelsdorf core (Fig. 5B). For these reasons, accurate correlations are possible only within the lower 50-75% of the black shale facies of each shale member, i.e., to ca. 30-33 cm in the Hushpuckney Shale (Fig. 5A) and to ca. 28-31 cm in the Stark Shale (Fig. 5B).

The laminated black shales facies of Heilman Stark differs considerably in thickness and composition relative to the other three Stark Shale study units, despite being located only 40 km south of the Ermal and Womelsdorf cores. Differences in the character of alternating dm-thick Corg-rich and -poor layers make correlation of the Heilman core with other locales tentative at all stratigraphic levels. The correlation scheme in Figure 5B was chosen because it (1) represents the best one-to-one match with dm-scale Corg couplets in other Stark units, (2) aligns phosphate nodule sets of similar character, and (3) yields thickness changes consistent with regular variation in sedimentation rates in the Heilman core relative to other Stark units. These correlations imply (1) strong condensation of the basal 5 cm of Heilman Stark, (2) more rapid sedimentation (ca. 25-30% faster) of Heilman Stark above 10 cm than of the correlative portions of other Stark units, and (3) synchronous onset and quasi-synchronous termination of anoxia throughout the study area (Fig. 5B). Alternative correlations without basal condensation of Heilman Stark are less likely owing to (1) an implied lack of regional synchroneity of the anoxic event, and (2) irregular variation in thickness of layers in the Heilman core relative to other Stark units. Stratigraphic differences in Heilman Stark may be attributable to its proximity to the southern margin of the Eastern Midcontinent Shelf (Fig. 1).

Fine-scale correlation of the study units permits inferences regarding sedimentation rates. Absolute sedimentation rates are not known but presumed to be very slow on the basis of thin laminae (<<1 mm), abundant phosphate, and high concentrations of trace metals and normally rare pelagic fossils (Coveney et al. 1989; Watney et al. 1995). Variation in relative sedimentation rates between study units may be inferred on the basis of lateral changes in the thickness of correlatable, cm- to dm-thick layers. In the Hushpuckney Shale, individual layers vary in thickness by <±30% over distances of 150 km (Fig. 5A), whereas in the Stark Shale, individual layers vary in thickness by <±10% at 0-18 cm, increasing to <±40% at >18 cm (Fig. 5B; n.b., excluding the Heilman core). Limited lateral thickness variation implies either uniform or synchronously variable sedimentation rates across the study area during deposition of the study shales (except for the Heilman Stark). Temporal variation in sedimentation rates may be inferred from vertical changes in the thickness of dm-scale compositional cycles. Assuming a quasi-periodic forcing mechanism, the relatively uniform thickness of such cycles implies that sedimentation rates were approximately constant at the timescales associated with cycle deposition; this does not preclude sedimentation rate variation at shorter timescales. Generally thicker cycles in the uppermost 20-30% of the black shale facies of many study units (not shown) suggest an increase in sedimentation rates as water-column stratification broke down and a transition to bioturbated gray shales occurred.

Spatio-Temporal Variation In Major Components

Organic component parameters exhibit pronounced patterns of interformational and lateral variation (Hoffman et al. 1997). Organic carbon abundance, as proxied by TC, (1) is greatest in the Hushpuckney Shale and least in the Muncie Creek Shale, and (2) increases to the north in both the Hushpuckney and Stark shales. Organic matter in the study units is not homogeneous but consists of several maceral types, primarily vitrinite (Vt; 26±12 vol%) and inertinite (In; 12±9 vol%), which occur in thin, elongate, internally structured bands (<1.5 x 2-80 µm and <0.5 x 2-40 µm, respectively) or as macerated fragments (i.e., vitrodetrinite and inertodetrinite), and which are probably derived from higher land plants. In/Vt ratios (1) exhibit the lowest values in the Stark Shale and the highest values in the Muncie Creek Shale (n.b., based on Edmonds core), and (2) decrease to the north (<0.4 in Edmonds) and increase to the south (0.9-1.1 in Heilman; n.b., based on Stark Shale; Fig. 8A). Bulk organic $\delta^{13}C$ values (1) are significantly lower in the Hushpuckney Shale (-28.3±0.8 ‰ PDB) than in the Stark and Muncie Creek shales (-27.6±0.5 and -27.4±0.3 ‰ PDB, respectively), and (2) exhibit no obvious lateral trends (Fig. 8B). Only minor amounts (< 1 vol%) of marine-derived macerals (e.g., telalginite) were observed, and bulk organic $\delta^{13}C$ values are consistent with organic matter of degraded terrigenous rather marine algal origin, which would be expected to yield more ^{13}C-depleted C-isotopic compositions (Lewan 1986; cf. Maynard 1981).

Trace-element degree-of-anoxia (DOA) indices and authigenic component abundances also exhibit pronounced spatio-temporal variation. In the study units, the best DOA proxies are redox-sensitive trace-element ratios, e.g., Mo/TC, U/TC, V/Cr, and V/(V+Ni) (Hoffman et al. 1997; cf. Lewan and Maynard 1982; Anderson et al. 1989; Jones and Manning 1994; n.b., all indices normalized on a per-unit carbon basis owing to the organic affinity of these elements). These DOA indices (1) are greatest in the Stark Shale and least in the Muncie Creek Shale, and (2) increase to the north in both the Hushpuckney and Stark shales, indicating stronger bottomwater anoxia in that direction (Fig. 9A). With regard to authigenic components, Fe-sulfide abundance (as proxied by TS) (1) is greatest in the Stark Shale and least in the Muncie Creek Shale, and (2) increases to the north in both the Hushpuckney and Stark shales (Hoffman et al. 1997). Phosphate abundance (as proxied by P_2O_5) (1) is greatest in the Hushpuckney Shale and least in the Muncie Creek Shale, and (2) exhibits a complex pattern of lateral variation, increasing northward in the Hushpuckney Shale and southward in the Stark Shale (Fig. 9B).

Detrital components of the study units exhibit pronounced lateral gradients but little variation between shale members. Strong co-variation of $Al_2O_3^*/SiO_2^*$ with K_2O^* and TiO_2^* (Fig. 7A-B) supports the inference of a two-component mixing system dominated by smectite (or mixed-layer I/S) and illite (see above), and regional variation in detrital-element parameters indicates dominance of the smectitic phase to the south and a more variable clay-mineral assemblage with a larger proportion of the illitic phase to the north (Fig. 7C). Because study units to the south have been buried somewhat more deeply than those to the north (Watney et al. 1989), it is unlikely that these mineralogic differences are due to diagenetic factors (e.g., smectite-to-illite transformation; cf. Grim 1968), which would have enhanced illite abundances in the south. Rather, the northern fraction probably represents illite of detrital origin and the southern fraction a detrital smectite or diagenetically altered mixed-layer I/S phase.

Interformational and lateral differences in bulk composition between study units can be investigated by calculating volumetric fractions for the major components. Component volumes were based on (1) mean concentrations of the elemental proxies (TC, TS, and P_2O_5) for the non-clastic components (organic carbon, Fe-sulfide, and phosphate, respectively), (2) conversion of proxy concentration to component mass using weight ratios (i.e., 1.2 for Corg:TC, 1.87 for FeS_2:TS, and 2.37 for $Ca_5(PO_4)_3F:P_2O_5$), (3) conversion of component masses to volumes using mean density values (i.e., 1.1, 5.2, 3.2, and 2.6 g cm^{-3}, for organic carbon, Fe-sulfide, phosphate, and clay minerals, respectively), (4) estimation of dominant clay-mineral volumes based on total clay volume, unit-mean $Al_2O_3^*/SiO_2^*$ ratios (Fig. 7C), and assumed endmember $Al_2O_3^*/SiO_2^*$ ratios of 0.30 and 0.65 for smectite and illite, respectively, and (5) estimation of organic maceral volumes based on total organic volume and relative point-count frequencies for each maceral type (Fig. 8A). These calculations reveal that (1) the volumetric fraction of illite (I) increases and that of smectite (S) decreases northward (e.g., from 10% I/58% S at Heilman Stark to 34% I/34% S at Edmonds Stark), and (2) the volumetric fraction of vitrinite (Vt) increases and that of inertinite (In) decreases northward (e.g., from 7% Vt/10% In at Heilman Stark to 18% Vt/4% In at Edmonds Stark; Fig. 10). Because the correlatable lower 50-75% of the laminated black shale facies of each shale member exhibits minimal lateral thickness variation (±5%, except for Heilman Stark; Fig. 5), bulk sedimentation rates for the Hushpuckney and Stark shales were roughly uniform across the study area. Thus, large lateral differences in fractional component volumes (Fig. 10) document an inverse relation in the bulk accumulation rates of the dominant clay minerals and organic macerals. This suggests that two sediment fluxes with different transport vectors, i.e., a northern illite- and vitrinite-rich flux and a southern smectite- and inertinite-rich flux, were intermingled within the study area.

Covariation Between Major Components

Elemental proxies for some of the major components exhibit significant covariation that may comment on environmental conditions and processes. Elemental proxies for the major components exhibit only two significant correlations ($p(\alpha) <.05$): (1) TC covaries positively with Al_2O_3*/SiO_2*, and (2) P_2O_5 covaries negatively with Al_2O_3*/SiO_2* (Table 2). Covariation of TC and Al_2O_3*/SiO_2* is non-linear (exhibiting a distinct change of slope at ca. 25 wt% TC) and strong (r^2 = 0.81, based on a second-order polynomial fit; Fig. 11A). Covariation of P_2O_5 with Al_2O_3*/SiO_2* is weaker, although a sharp division exists between samples with high Al_2O_3*/SiO_2* ratios (ca. >0.5), which yield uniformly low P_2O_5 values, and those with low Al_2O_3*/SiO_2* ratios (ca. <0.5), which yield variably low to high P_2O_5 values (Fig. 12). Whereas TC-Al_2O_3*/SiO_2* covariation is likely to comment significantly on relations between organic and clastic fluxes, P_2O_5-Al_2O_3*/SiO_2* covariation may represent a spurious association that depends largely on the relationship of both parameters to organic carbon (see Discussion below).

Although other major component pairs did not yield significant correlations (Table 2), some patterns of component covariation may nonetheless provide significant environmental information. First, TC-TS values fall well below the "normal" trend for oxic-suboxic marine environments (Berner and Raiswell 1983) and exhibit a large, positive regression Y-intercept (1.8 wt% TS; Fig. 11B). These observations are consistent with strong anoxia during deposition of the study units as well as with Fe-limited conditions of authigenic pyrite formation (Hoffman et al. 1997; cf. Lyons and Berner 1992). Second, TC exhibits a complex relationship with P_2O_5, in which samples with low (<15 wt%) or high (>32 wt%) TC concentrations yield uniformly low P_2O_5 values and those with intermediate TC concentrations (15-32 wt%) yield variably low to high P_2O_5 values (Fig. 11C). Also, molar C/P ratios exhibit a trimodal distribution with modes at high (C/P_{mol} = 600-1500), intermediate (C/P_{mol} = 100-150), and low ratios (C/P_{mol} = 15-40; Fig. 13). These patterns are virtually identical for both the Hushpuckney and Stark shales, implying an origin in recurrent depositional or diagenetic processes and not as an artefact of data distribution (see Discussion below).

In the organic fraction, patterns of covariation between total organic carbon (TOC) concentrations, maceral types, and C-isotopic compositions may provide insights on the nature and origin of organic matter in the study units. Vitrinite (Vt) and inertinite (In) vary in relative abundance (e.g., inertinite/vitrinite ratio) as a function of TOC (as proxied by inertinite+vitrinite, i.e., total volumetric fraction of organic macerals; Fig. 8A). Positive covariation of In/Vt and TOC is observed in the Edmonds core for all three shale members ($r^2 = 0.66\text{-}0.96$; $p(\alpha) <.05$). Organic carbon $\delta^{13}C$ values also tend to covary positively with TOC, e.g., in the Muncie Creek and Hushpuckney shales, but not in the Stark Shale (Fig. 8B). These observations suggest that (1) each maceral type has a distinct C-isotopic composition (inertinite = -26.1 to -27.1 ‰; vitrinite = -27.9 to -29.1 ‰), (2) bulk organic C-isotopic values represent a mass-weighted average of the endmember compositions, and (3) fluxes of vitrinite and inertinite were at most weakly coupled, reflecting different transport vectors or intensities (Hoffman et al. 1997).

DISCUSSION

Environmental Conditions & Processes

The fine-scale stratigraphic correlations and compositional patterns documented above are invaluable for understanding environmental conditions and processes in the study units and controls on spatio-temporal variation thereof. With few exceptions (as noted above), patterns of covariation among major component proxies were the same for all four sampling dimensions (e.g., Fig. 4). Especially significant for environmental interpretations are similar patterns of covariation in the lateral (Figs. 7-12) and intracyclic dimensions (Fig. 2 of Algeo et al., companion paper). This similarity implies that fine-scale compositional variation within the study units was due to processes that had a strong geographic expression, e.g., that the gradients of critical environmental parameters fluctuated laterally across the Eastern Midcontinent Shelf at timescales associated with the deposition of dm-scale compositional cycles.

Stratification patterns revealed by X-radiography constrain some aspects of environmental conditions within the Midcontinent Seaway. Deposition of thin, continuous sediment layers over wide areas (e.g., as documented by cm-scale correlations; Fig. 5) requires uniformity of environmental conditions and synchroneity of changes in water-column chemistry throughout the 200-km-long study area, probably due to existence of a strong pycnocline and a well-mixed bottomwater layer (cf. Lyons 1991). Such uniform conditions suggest water depths in excess of storm wave base (>100 m?), which are also consistent with a lack of evidence of syndepositional erosion (see below). Bottomwater conditions remained widely uniform during deposition of the lower 70-80% of each black shale member but became increasingly variable on a local scale as water-column stratification broke down, which is reflected in an increase in variability of the thickness and composition of the upper 25-50% of each study unit (Fig. 5).

In most anoxic marine systems, bottomwater oxygen depletion is promoted by water-column stratification (Demaison and Moore 1980; Arthur and Sageman 1994). In the Midcontinent Seaway, stratification may have resulted from quasi-estuarine circulation, leading to development of a strong proximal halocline to the north and a weak distal thermocline to the south (Heckel 1977, 1991; Desborough et al. 1991). A regional halocline may have been sustained either by freshwater runoff from the peri-equatorial Appalachian Mountains, forming a hyposaline surfacewater layer, or by dissolution of subaqueously-exposed evaporites (e.g., in the Williston Basin), forming a hypersaline bottomwater layer (Schutter 1983; Hatch and Leventhal 1992). Salinity stratification is promoted by a microtidal range and strong surfacewater runout, minimizing mixing with and entrainment of saline deepwaters (Dyer 1995), conditions that are characteristic of large, semi-restricted seaways (cf. Bay of Bengal; Ittekkot et al. 1992). Although a thermocline might have been sufficient to account for regional stratification within the Midcontinent Seaway, strongly directional surfacewater influx would have favored halocline development. Evidence of directional surfacewater influx is provided by a pronounced lateral gradient in DOA indices, reflecting greater bottomwater oxygen depletion to the north (Fig. 9A; Hoffman et al. 1997), consistent with a stronger pycnocline in proximal portions of the Midcontinent Seaway (e.g., Heckel 1977, 1991; Desborough et al. 1991).

Water circulation patterns may also be inferred from patterns of clastic flux. In the study units, regional variation in clay-mineral abundance (Fig. 7C) reflects dominance of an illitic phase to the north and a smectitic phase to the south, which may be accounted for by either (1) a two-source model, in which illite was northern-derived and smectite southern-derived, or (2) a differential rainout rate model, in which clastics were largely northern-derived and illite settled out of suspension more rapidly than smectite (Fig. 14). Factors constraining the viability of these two models are (1) minimal lateral thickness variation within the correlatable lower 50-75% of each shale member (Fig. 5), indicating regionally uniform bulk sedimentation rates, and (2) an inverse lateral relationship in the volumetric fractions of illite and smectite (Fig. 10), implying that bulk *mineral* accumulation rates increased northward for illite and southward for smectite. These considerations favor the two-source model, i.e., a northern illite-dominated clastic flux, probably associated with a low-salinity surfacewater vector, and a southern smectite-dominated clastic flux, probably associated with upwelling of deepwater from the Anadarko Basin (cf. Naidu and Mowatt 1983). Wholesale trapping of sediment in modern estuaries is due in large measure to their well-mixed state; stratified estuarine systems exhibit much lower "filter efficiencies" (i.e., the ratio of sediment accumulation to fluvial sediment input) owing to reduced flocculation of charged clastic particles (e.g., clays; Dyer 1995).

Prounounced covariation between clay-mineral abundances and organic carbon concentrations implies strong coupling between the processes responsible for clastic transport and organic matter accumulation. Co-transport of siliciclastics and organic matter via a water-borne vector is likely because (1) organic carbon correlates strongly with illite abundance (Fig. 11A) and, hence, with greater surfacewater influx (see above), and (2) the dominant organic macerals in the study units (i.e., inertinite and vitrinite) are refractory material of terrigenous origin. As with relative clay-mineral abundances (see above), lateral gradients in inertinite/vitrinite (In/Vt) ratios (Fig. 8A) may be accounted for by either a two-source model or a differential rainout rate model. Relevant factors include (1) regionally uniform bulk sedimentation rates; and (2) an inverse lateral relationship in the volumetric fractions of inertinite (In) and vitrinite (Vt; Fig. 10), indicating that bulk *maceral* accumulation rates increase northward for vitrinite and southward for inertinite. Thus, the two-source model also may apply to organic maceral fluxes, i.e., a northern vitrinite-dominated flux and a southern inertinite-dominated flux. Although relative maceral abundances are potentially also influenced by environmental factors that could induce differential rates of oxidation (e.g., Westrich and Berner 1984; Hedges et al. 1988), distal increases in bulk inertinite accumulation rates are unlikely to be explained by this mechanism.

Sediment-starved conditions, reflecting slow accumulation rates for both clastics and organic matter, generally imply control of spatio-temporal variation in sediment composition through a dilution process. The nature of this dilution process, which can be due to variation in either clastic or organic fluxes, may be constrained in the study units by the observations above. Proximal-to-distal dilution ratios are similar for clay-mineral and organic maceral abundances, i.e., both $(I/S)_{prox}/(I/S)_{dist}$ and $(Vt/In)_{prox}/(Vt/In)_{dist}$ equal about six (cf. Fig. 10). In other words, the ratio of the northern-derived (illite-, vitrinite-rich) sediment flux to the southern-derived (smectite-, inertinite-rich) sediment flux is about six times larger at proximal locales (e.g., Edmonds Stark) than at distal locales (e.g., Heilman Stark). The northern-derived sediment flux is probably the more variable in absolute magnitude because detrital and organic component proxies exhibit substantially greater variability at proximal locales than at distal ones (Figs. 7C, 8A). Because surfacewater fluxes are generally more variable than deepwater fluxes (at timescales of ca. 10^2-10^5 y), this observation is consistent with a northern-derived surfacewater mass in the Midcontinent Seaway. Association of higher TOC concentrations with greater surfacewater influx in the study units represents an *organic* dilution process that reflects the predominantly terrigenous source of the organic matter (cf. Aplin et al. 1992; Ittekkot et al. 1992). This pattern is the converse of controls on compositional variation in Appalachian Devonian black shales, in which lower (higher) TOC values correlate with increased (reduced) influx of clastics and low-salinity surfacewaters, representing a *clastic* dilution process that reflects the predominantly marine source of the organic matter (Jaminski et al. 1997).

Despite slow sedimentation rates, no intraformational erosion occurred in the study area, as evidenced by (1) lack of mechanical dislocation or abrasion of phosphate nodules (cf. Kidder 1985;

Kidder et al. 1996), and (2) minimal lateral variation in the thickness of correlatable layers (Fig. 5; n.b., thickness variation in Heilman Stark probably due to basal condensation rather than intraformational erosion). Thus, bottom currents were weak or absent in the study area, unlike in modern continent-margin upwelling zones, in which longshore and cross-shelf currents contribute to winnowing and concentration of authigenic phosphate in surface sediments and interfere with development of thin, laterally extensive sediment layers (Bailey 1991; Smith 1992; Glenn et al. 1994). Rather, stratification patterns in the study units more closely resemble those encountered in restricted anoxic basins such as the modern Black Sea, in which cm-thick layers are laterally continuous over 100s of kilometers (Lyons 1991; Repeta 1993). To the south, in southeastern Kansas and northeastern Oklahoma, the Stark Shale is reported to be discontinuous over local paleotopographic highs on which only a thin phosphatic, conodont-bearing lag is present, suggesting possible upwelling-induced current winnowing in deeper slope environments (Schutter 1983; Heckel, manuscript).

Controls on Authigenic Phosphate Formation

Phosphorus fluxes in marine systems are closely linked to redox conditions and organic matter cycling, and the distribution of phosphate in the study units may provide information regarding such processes. Formation of authigenic phosphate (i.e., carbonate fluorapatite, or francolite) depends on the generally transient co-occurrence of a number of factors. Modern phosphates form primarily in offshore areas of high primary productivity, i.e., where the flux of sedimentary organic matter substantially exceeds that of clastic detritus (Burnett 1980; Burnett et al. 1982). Supersaturation of sediment porewaters with respect to francolite commonly occurs only within a narrow zone in the shallow subsurface where upward-diffusing PO_4^{3-} and CO_3^{2-} released from decaying organic matter mix with downward-diffusing Ca^{2+}, SO_4^{2-} and F^- from the overlying water column (Fig. 15). Precipitation occurs mainly at depths of 5-20 cm below the sediment-water interface and is favored by oxygen-depleted, mildly alkaline conditions, such as commonly develop in the NO_3^- reducing zone (Krom and Berner 1980; Martens 1993; Jarvis et al. 1994). A critical factor in the retention and concentration of sedimentary P may be Fe cycling in association with redox changes within the sediment. Given weakly oxic conditions at or just below the sediment-water interface, iron oxyhydroxides (FeOOH) are precipitated as a solid phase that scavenges dissolved PO_4^{3-} from porewaters (Fig. 15). Following burial to depths at which porewaters become anoxic, dissolution of iron oxyhydroxides under reducing conditions liberates both Fe and adsorbed P, which diffuse upward to be reprecipitated in the oxic zone. Redox-related Fe cycling retains P within the shallow subsurface, allowing sufficient time for ionic diffusion and slow growth of phosphate nodules (Burnett et al. 1982). Thus, phosphate precipitation is most favored under weakly anoxic conditions (Jarvis et al. 1994), an inference supported by high abundances of phosphate nodules at the upper and lower boundaries of the oxygen minimum zone on modern continental shelves at dissolved O_2 levels of ca. 0.1-0.2 ml l^{-1} (Burnett 1980).

This model may offer insights regarding controls on P fluxes within Midcontinent Pennsylvanian offshore black shales. In the study units, authigenic phosphate nodules precipitated in the shallow subsurface and were not subsequently affected by transport or current winnowing (Fig. 5; Kidder 1985; Kidder et al. 1996; Hoffman et al. 1997). The present distribution of phosphate in the study units and its relations to other major components (especially Corg) are complex. First, X-radiographic evidence of preferential development of nodules near the upper and lower contacts of organic-rich layers (Fig. 5) suggests a redox control on phosphate precipitation, probably in association with an outward flux of P from within high-TOC layers. This also implies fluctuations in porewater oxygen levels at a centimeter scale in the shallow subsurface environment (cf. Hatch and Leventhal 1992).

Second, molar C/P ratios may comment on organic matter sources and/or diagenetic fluxes of P in the study units (Froelich et al. 1988; Berner et al. 1993). Although the high, intermediate, and low C/P_{mol} modes (i.e., 600-1500, 100-150, and 15-40; Fig. 13) are close to those for higher land plants, marine phytoplanton (106 = Redfield ratio), and bacterial biomass, respectively (Redfield et al. 1963; Delwiche and Likens 1977; Vadstein et al. 1988), a lack of petrographic evidence for any significant quantity of algal- or bacterial-derived organic matter (e.g., alginite or bituminite) suggests that the present frequency distribution of C/P_{mol} ratios is of secondary rather than primary origin. In particular, the low C/P_{mol} mode (15-40) represents samples containing macroscopic phosphate nodules, and formation-mean C/P_{mol} ratios (26.2 for Hushpuckney, 49.8 for Stark, and 108.6 for Muncie Creek) reflect the relative prevalence of nodules in the three shale members. The mean C/P_{mol} ratio for all samples (40.2) is significantly lower than that of either terrigenous or marine sources of organic matter, requiring either (1) preferential regeneration of organic carbon, which is at odds with recent studies demonstrating more rapid bacterial cycling of organic P (Ingall et al. 1993), or (2) a large non-organic P flux, e.g., from detrital Fe-oxyhydroxides or apatite (Berner et al. 1993).

Third, the complex relationship of phosphate and organic matter, in which samples with low or high TC yield low P_2O_5 values and those with intermediate TC yield variably low to high P_2O_5 values (Fig. 11C), cannot be attributed to different types of organic matter in each sample group because compositional variation within the organic component is limited and linearly related to TOC concentration (Fig. 8A). Rather, patterns of TC-P_2O_5 covariation are likely to reflect redox controls, i.e., a non-linear response of processes responsible for P accumulation to changes in bottomwater oxygen levels. For example, (1) high TC-low P_2O_5 samples may record strongly anoxic conditions, favoring the ferrous ion Fe^{2+} and limiting the potential for redox cycling of iron and retention of PO_4^{3-}, (2) intermediate TC-high P_2O_5 values may record weakly anoxic conditions, promoting redox cycling of iron (between the Fe^{2+} and Fe^{3+} states) and retention of PO_4^{3-}, and (3) low TC-low P_2O_5 values may record more-oxygenated conditions, favoring the ferric ion Fe^{3+} and limiting redox cycling of iron and retention of PO_4^{3-} (Fig. 15; Glenn et al. 1994; Jarvis et al. 1994). This hypothesis requires strong coupling between Corg concentrations and bottomwater oxygen levels, which is consistent with TC-DOA correlations in the study units (Hoffman et al. 1997).

Lastly, interformational and regional trends in phosphate abundance are related to patterns of spatio-temporal variation in DOA indices. Bottomwater oxygen levels are lowest in the Stark Shale and highest in the Muncie Creek Shale, and oxygen levels decrease northward in both the Hushpuckney and Stark shales (Fig. 9A; Hoffman et al. 1997). P_2O_5 values in these two shales are similar at southern locales (ca. 3-4 wt%) but diverge northward, increasing to >6 wt% in Edmonds Hushpuckney and decreasing to <1 wt% in Edmonds Stark (Fig. 9B; n.b., Edmonds Muncie Creek also exhibits low P_2O_5 values). These patterns are consistent with redox control of phosphate formation provided that (1) maximum P retention occurs under weakly anoxic conditions (i.e., low but measurable oxygen levels), and (2) bottomwater oxygen levels were more variable in the Hushpuckney Shale than in the Stark Shale, especially in the northern part of the study area (Fig. 9B). Note that this pattern is consistent with a combination of non-linear TC-P_2O_5 covariation

(Fig. 11C) and an inferred linear relation between DOA and Corg content (see above).

In summary, these observations suggest that P accumulation in the study units was controlled by a combination of sedimentation rates and redox conditions. The optimal conditions for authigenic phosphate formation were slow sedimentation rates, permitting downward diffusion of seawater PO_4^{3-} and slow nodule growth, and low but variable oxygen levels (i.e., weakly anoxic conditions, ca. 0.1-0.2 ml O_2 l^{-1} H_2O), permitting retention of PO_4^{3-} through redox cycling of iron oxyhydroxides (Fig. 15). Sedimentation rates and redox conditions in the Midcontinent Seaway were, in turn, a function of clastic fluxes and pycnocline strength (itself dependent on surfacewater flux; see above).

Control of phosphogenesis primarily by slow sedimentation rates and porewater redox conditions differs from the model of Heckel (1977, 1991), which invoked upwelling of nutrient-rich deepwaters and enhanced primary productivity in the Midcontinent Seaway on the basis of high TOC and P_2O_5 concentrations in offshore black shales. This model does not accord well with observations from the study units because (1) the preserved organic matter is overwhelmingly of terrigenous rather than marine origin, (2) Fe-sulfides are strongly ^{34}S-depleted relative to contemporary seawater sulfate ($\Delta^{34}S$ = -40±5 ‰; Coveney and Shaffer 1988), providing no evidence of the high SO_4^{-2} reduction rates that typically accompany rapid deposition of labile organic matter (Goldhaber and Kaplan 1974), and (3) evidence is lacking for current reworking of sediments, which is necessary for concentration of phosphate in areas of moderate to high sedimentation rates (e.g., as in modern continental-margin upwelling zones). Further, TOC is generally a poor proxy for primary productivity (Wignall 1994), and high TOC values in the study units are more likely due to a combination of low sedimentation rates, an *organic* dilution mechanism, and the refractory nature of terrigenous organic matter.

The best modern analog for the Midcontinent Seaway may be humid coastal estuaries subject to low clastic influx (Officer et al. 1984; Rabalais et al. 1991). At a broader geographic scale, the Midcontinent Seaway was semi-restricted (Heckel 1991) and, perhaps, analogous in this regard to silled anoxic basins such as the Black Sea, which are characterized by a regionally strong pycnocline and low primary productivity (Demaison and Moore 1980; Wignall 1994). In contrast, modern continental margins subject to western-boundary upwelling, such as the Peruvian and Namibian shelves, tend to exhibit laterally variable pycnocline strength and high primary productivity (Demaison and Moore 1980; Arthur and Sageman 1994). Western-boundary upwelling, related to offshore Ekman transport of surfacewaters, might have been possible in the Midcontinent Seaway from a paleogeographic perspective (Heckel 1991), but stratigraphic and geochemical observations from the study units offer little support for this inference. If upwelling was operative in the Midcontinent Seaway, its intensity must have been considerably lower than on modern western-boundary continental margins (Heckel, manuscript, pers. comm. 1996).

CONCLUSIONS

Upper Pennsylvanian offshore shales were deposited in the Midcontinent Seaway under sediment-starved conditions beneath a strong proximal halocline subject to fluctuations in intensity. The clastic fraction of the shales consists of an illite-rich component associated with influx of low-salinity surfacewaters from continental areas to the north, and a smectite-rich component associated with upwelling of deepwaters from the Anadarko Basin to the south. The organic component of the shales is composed largely of macerals of terrigenous origin (inertinite and vitrinite) and covaries strongly with the clastic fraction, i.e., higher TOC values and lower inertinite/vitrinite ratios correlate with the illite-rich component. Greater compositional variation at proximal (northern) locales suggests a temporally variable surfacewater flux, and association of higher concentrations of terrigenous-derived organics with greater surfacewater influx implies control of sediment composition by an *organic* dilution process. Correlation of cm-thick layers across the 200-km-long study area and absence of evidence of intraformational erosion and winnowing indicate widely uniform sub-pycnocline conditions and a lack of strong bottom currents. Authigenic phosphate was precipitated preferentially along the upper and lower contacts of high-TOC layers and in areas of low but fluctuating bottomwater oxygen levels (i.e., ca. 0.1-0.2 ml O_2 l^{-1} H_2O, or weakly anoxic conditions). Slow sedimentation rates were critical to phosphate formation, permitting downward diffusion of seawater PO_4^{3-} and slow growth of nodules. Upwelling intensity in the Midcontinent Seaway was weak and evidence for upwelling-enhanced primary productivity is lacking.

ACKNOWLEDGMENTS

We wish to thank Mark Thompson (Kentucky Geological Survey) for analytical assistance, Lisa Trump (University of Cincinnati) for drafting services, and Phil Heckel (University of Iowa) for helpful discussions and manuscript reviews. All cores were drilled and supplied by the Kansas Geological Survey (KGS series).

REFERENCES

ALGEO, T.J., AND WOODS, A.D., 1994, Microstratigraphy of the Lower Mississippian Sunbury Shale: A record of solar-modulated climatic cyclicity: Geology, v. 22, p. 795-798.

ALGEO, T.J., PHILLIPS, M., JAMINSKI, J., AND FENWICK, M., 1994, High-resolution X-radiography of laminated sediment cores: Journal of Sedimentary Research, v. A64, p. 665-668.

ANDERSON, R.F., FLEISHER, M.Q., AND LEHURAY, A.P., 1989, Concentration, oxidation state, and particulate flux of uranium in the Black Sea: Geochim. Cosmochim. Acta, v. 53, p. 2215-2224.

APLIN, A.C., BISHOP, A.N., CLAYTON, C.J., KEARSLEY, A.T., MOSSMANN, J.-R., PATIENCE, R.L., REES, A.W.G., AND ROWLAND, S.J., 1992, A lamina-scale geochemical and sedimentological study of sediments from the Peru Margin (Site 680, ODP Leg 112), *in* C.P. Summerhayes, W.L. Prell, and K.C. Emeis, eds., Upwelling Systems: Evolution Since the Early Miocene: Geol. Soc. London Spec. Publ. 64, p. 131-149.

ARBENZ, J.K., 1989, The Ouachita System, *in* A.W. Bally and A.R. Palmer, eds., The Geology of North America--An Overview (v. A), Geological Society of America, Boulder, Colorado, p. 371-396.

ARTHUR, M.A., AND SAGEMAN, B.B., 1994, Marine black shales: A review of depositional mechanisms and significance of ancient deposits: Ann. Rev. Earth Planet. Sci., v. 22, p. 499-551.

BAILEY, G.W., 1991, Organic carbon flux and development of oxygen deficiency on the modern Benguela continental shelf south of 22°S: Spatial and temporal variability, *in* Tyson, R.V., and Pearson, T.H., eds., Modern and Ancient Continental Shelf Anoxia: Geological Society of London Special Publication 58, p. 171-183.

BERNER, R.A., AND RAISWELL, R., 1983, Burial of organic carbon and pyrite sulfur in sediments over Phanerozoic time: A new theory: Geochim. Cosmochim. Acta, v. 47, p. 855-862.

BERNER, R.A., RUTTENBERG, K.C., INGALL, E.D., AND RAO, J.-L., 1993, The nature of phosphorus burial in modern marine sediments, *in* R. Wollast, F.T. Mackenzie, and L. Chou, eds., Interactions of C, N, P and S Biogeochemical Cycles and Global Change, NATO ASI Series v. 14: Berlin, Springer, p. 365-

378.

Biscaye, P.E., 1965, Mineralogy and sedimentation of Recent deep-sea clay in the Atlantic Ocean and adjacent seas and oceans: Geol. Soc. Am. Bull., v. 76, p. 803-831.

Boardman, D.R., II, and Heckel, P.H., 1989, Glacial-eustatic sea-level curve for early Late Pennsylvanian sequence in north-central Texas and biostratigraphic correlation with curve for midcontinent North America: Geology, v. 17, p. 802-805.

Burnett, W.C., 1980, Apatite-glauconite associations off Peru and Chile: Palaeo-oceanographic implications: J. Geol. Soc. London, v. 137, p. 757-764.

Burnett, W.C., Beers, M.J., and Roe, K.K., 1982, Growth rates of phosphate nodules from the continental margin off Peru: Science, v. 215, p. 1616-1618.

Calvert, S.E., Bustin, R.M., and Ingall, E.D., 1996, Influence of water column anoxia and sediment supply on the burial and preservation of organic carbon in marine shales: Geochim. Cosmochim. Acta, v. 60, p. 1577-1593.

Canfield, D.E., 1994, Factors influencing organic carbon preservation in marine sediments: Chemical Geology, v. 114, p. 315-329.

Chu, T.-H., Bonnell, L.M., and Anderson, T.F., 1993, Speciation and isotopic composition of sulfur in the Oxford Clay Formation (Jurassic, U.K.): Chem. Geol., v. 107, p. 443-445.

Coveney, R.M., Jr., and Shaffer, N.R., 1988, Sulfur-isotope variations in Pennsylvanian shales of the midwestern United States: Geology, v. 16, p. 18-21.

Coveney, R.M., Jr., Watney, W.L., and Maples, C.G., 1989, Rates and durations for the accumulation of Pennsylvanian black shales in the midwestern United States: Kansas Geological Survey, Subsurface Geology Series 12, p. 73-76.

Crowell, J.C., 1978, Gondwanan glaciation, cyclothems, continental positioning, and climate change: American Journal of Science, v. 278, p. 1345-1372.

Crowley, T.J., Hyde, W.T., and Short, D.A., 1989, Seasonal cycle variations on the supercontinent of Pangaea: Geology, v. 17, p. 457-460.

Crowley, T.J., Yip, K.-J., Baum, S.K., and Moore, S.B., 1996, Modelling Carboniferous coal formation: Paleoclimates, v. 2, p. 159-177.

Delwiche, C.C., and Likens, G.E., 1977, Biological response to fossil fuel combustion products, *in* W. Stumm, ed., Global Chemical Cycles and Their Alterations by Man: Berlin, Dahlem Konferenzen, p. 73-88.

Demaison, G.J., and Moore, G.T., 1980, Anoxic environments and oil source bed genesis: Org. Geochem., v. 2, p. 9-31.

Desborough, G.A., Hatch, J.R., and Leventhal, J.S., 1991, Geochemical and mineralogical comparison of the Upper Pennsylvanian Stark Shale Member of the Dennis Limestone, east-central Kansas, with the Middle Pennsylvanian Mecca Quarry Shale Member of the Carbondale Formation in Illinois and of the Linton Formation in Indiana: U.S. Geological Survey Circular 1058, p. 12-30.

Dyer, K.R., 1995, Sediment transport processes in estuaries, *in* G.M.E., Perillo, ed., Geomorphology and Sedimentology of Estuaries: Amsterdam, Elsevier, p. 423-449.

Ece, O.I., 1987, Petrology of the Desmoinesian Excello black shale of the midcontinent region of the United States: Clay and Clay Minerals, v. 35, p. 262-270.

Froelich, P.N., Arthur, M.A., Burnett, W.C., Deakin, M., Hendsley, V., Jahnke, R., Kaul, L., Kim, K.-H., Soutar, A., and Vathakanon, C., 1988, Early diagenesis of organic matter in Peru continental margin sediments: Phosphorite precipitation: Mar. Geol., v. 80, p. 309-343.

Glenn, C.R., Föllmi, K.B., Riggs, S.R., and 13 others, 1994, Phosphorus and phosphorites:

Sedimentology and environments of formation: Eclogae geologae Helvetiae, v. 87, p. 747-788.

GOLDHABER, M.B., AND KAPLAN, I.R., 1974, The sulfur cycle, in E.D. Goldberg, ed., The Sea: New York, Wiley, p. 569-655.

GRIM, R.E., 1968, Clay Mineralogy: New York, McGraw-Hill, 596 p.

HATCH, J.R., AND LEVENTHAL, J.S., 1992, Relationship between inferred redox potential of the depositional environment and geochemistry of the Upper Pennsylvanian (Missourian) Stark Shale Member of the Dennis Limestone, Wabaunsee County, Kansas, U.S.A.: Chemical Geology, v. 99, p. 65-82.

HAY, B.J., HONJO, S., KEMPE, S., ITTEKKOT, V.A., DEGENS, E.T., KONUK, T., AND IZDAR, E., 1990, Interannual variability in particle flux in the southwestern Black Sea: Deep-Sea Research, v. 37, p. 911-928.

HECKEL, P.H., 1977, Origin of phosphatic black shale facies in Pennsylvanian cyclothems of mid-contintent North America: American Association of Petroleum Geologists Bulletin, v. 61, p. 1045-1068.

HECKEL, P.H., 1986, Sea-level curve for Pennsylvanian eustatic marine transgressive-regressive depositional cycles along midcontinent outcrop belt, North America: Geology, v. 14, p. 330-334.

HECKEL, P.H., 1991, Thin widespread Pennsylvanian black shales of Midcontintent North America: A record of a cyclic succession of widespread pycnoclines in a fluctuating epeiric sea, *in* Tyson, R.V., and Pearson, T.H., eds., Modern and Ancient Continental Shelf Anoxia: Geological Society of London Special Publication 58, p. 259-273.

HECKEL, P.H., 1994, Evaluation of evidence for glacial-eustatic control over marine Pennsylvanian cyclothems in North America and consideration of possible tectonic effects, *in* Dennison, J.M., and Ettensohn, F.R., eds., Tectonic and Eustatic Controls on Sedimentary Cycles: SEPM (Society for Sedimentary Geology), Concepts in Sedimentology and Paleontology 4, p. 65-87.

HEDGES, J.I., CLARK, W.A., AND COWIE, G.L., 1988, Fluxes and reactivities of organic matter in a coastal marine bay: Limnol. Oceanogr., v. 33, p. 1137-1152.

HOFFMAN, D.L., ALGEO, T.J., MAYNARD, J.B., JOACHIMSKI, M.M., HOWER, J.C., AND JAMINSKI, J., in press, Microstratigraphic analysis of compositional variation in black shales: Offshore core shales in Upper Pennsylvanian cyclothems of the eastern Midcontinent Shelf (Kansas), USA, *in* Schieber, J., ed., Recent Progress in Shale Research: Stuttgart, Schweizerbart'sche.

HUTTON, A.C., 1987, Petrographic classification of oil shales: International Journal of Coal Geology, v. 8, p. 203-231.

INGALL, E.D., BUSTIN, R.M., AND VAN CAPPELLEN, P., 1993, Influence of water column anoxia on the burial and preservation of carbon and phosphorus in marine shales: Geochim. Cosmochim. Acta, v. 57, p. 303-316.

ITTEKKOT, V., HAAKE, B., BARTSCH, M., NAIR, R.R., AND RAMASWAMY, V., 1992, Organic carbon removal in the sea: The continental connection, *in* Summerhayes, C.P., Prell, W.L., and Emeis, K.C., eds., Upwelling Systems: Evolution Since the Early Miocene: Geological Society of London Special Publication 64, p. 167-176.

JAMINSKI, J., ALGEO, T.J., MAYNARD, J.B., AND HOWER, J.C., in press, Microstratigraphic analysis of compositional variation in black shales: The Cleveland Member of the Ohio Shale (Upper Devonian), central Appalachian Basin, USA, *in* Schieber, J., ed., Recent Progress in Shale Research: Stuttgart, Schweizerbart'sche.

JARVIS, I., BURNETT, W.C., NATHAN, Y., and 9 others, 1994, Phosphorite geochemistry: State-of-the-art and environmental concerns: Eclog. geol. Helv., v. 87, p. 643-700.

JOHNS, W.D., GRIM, R.E., AND BRADLEY, W.F., 1954, Quantitative estimations of clay minerals by diffraction methods: J. Sed. Pet., v. 24, p. 242-251.

JONES, B., AND MANNING, D.A.C., 1994, Comparison of geochemical indices used for the interpretation of palaeoredox conditions in ancient mudstones: Chem. Geol., v. 111, p. 111-129.

Kaplan, I.R., Emery, K.O., and Rittenberg, S.C., 1963, The distribution and isotopic abundance of sulphur in recent marine sediments off southern California: Geochim. Cosmochim. Acta, v. 27, p. 297-331.

Kidder, D.L., 1985, Petrology and origin of phosphatic nodules from the midcontinent Pennsylvanian epicontinental sea: J. Sed. Pet., v. 55, p. 809-816.

Kidder, D.L., Hussein, R.A.M., Mapes, R.H., and Eddy-Dilek, C.A., 1996, Regional diagenetic variation in maximum-transgrssion phosphates from Midcontinent Pennsylvanian shales, *in* Witzke, B.J., Ludvigson, G.A., and Day, J., eds., Paleozoic Sequence Stratigraphy: Views from the North American Craton: Boulder, Colorado, Geological Society of America Special Paper 306, p. 351-358.

Krom, M.D., and Berner, R.A., 1980, Adsorption of phosphate in anoxic marine sediments: Limnol. Oceanogr., v. 25, p. 797-806.

Lewan, M.D., 1986, Stable carbon isotopes of amorphous kerogens from Phanerozoic sedimentary rocks:Geochim. Cosmochim. Acta, v. 50, p. 1583-1591.

Lewan, M.D., and Maynard, J.B., 1982, Factors controlling the enrichment of vanadium and nickel in the bitumen of organic sedimentary rocks: Geochim. Cosmochim. Acta, v. 46, p. 2547-2560.

Lyons, T.W., 1991, Upper Holocene sediments of the Black Sea: Summary of Leg 4 box cores (1988 Black Sea Oceanographic Expedition), *in* Izdar, E., and Murray, J.W., eds., Black Sea Oceanography: Kluwer, Dordrecht, p. 401-441.

Lyons, T.W., and Berner, R.A., 1992, Carbon-sulfur-iron systematics of the uppermost deep-water sediments of the Black Sea: Chem. Geol., v. 99, p. 1-27.

Lyons, T.W., Berner, R.A., and Anderson, R.F., 1993, Evidence for large pre-industrial perturbations of the Black Sea chemocline: Nature, v. 365, p. 538-540.

Martens, C.S., 1993, Recycling efficiencies of organic carbon, nitrogen, phosphorus, and reduced sulfur in rapidly depositing coastal sediments, *in* R. Wollast, F.T. Mackenzie, and L. Chou, eds., Interactions of C, N, P and S Biogeochemical Cycles and Global Change, NATO ASI Series v. 14: Berlin, Springer, p. 379-400.

Maynard, J.B., 1981, Carbon isotopes as indicators of dispersal patterns in Devonian-Mississippian shales of the Appalachian Basin: Geology, v. 9, p. 262-265.

Mossmann, J.-R., Aplin, A.C., Curtis, C.D., and Coleman, M.L., 1991, Geochemistry of inorganic and organic sulphur in organic-rich sediments from the Peru Margin: Geochim. Cosmochim. Acta, v. 55, p. 3581-3595.

Naidu, A.S., and Mowatt, T.C., 1983, Sources and dispersal patterns of clay minerals in surface sediments from the continental-shelf areas off Alaska: Geol. Soc. Am. Bull., v. 94, p. 841-854.

Officer, C.B., Biggs, R.B., Taft, J.L., Cronin, L.E., Tyler, M.A., and Boyton, W.R., 1984, Chesapeake Bay anoxia: Origin, development, and significance: Science, v. 223, p. 22-27.

Parrish, J.T., 1993, Climate of the supercontinent Pangea: J. Geol., v. 101, p. 215-233.

Rabalais, N.N., Turner, R.E., Wiseman, W.J., Jr., and Boesch, D.F., 1991, A brief summary of hypoxia on the northern Gulf of Mexico continental shelf: 1985-1988, *in* Tyson, R.V., and Pearson, T.H., eds., Modern and Ancient Continental Shelf Anoxia: Geological Society of London Special Publication 58, p. 35-47.

Redfield, A.C., Ketchum, B.H., and Richards, F.A., 1963, The influence of organisms on the composition of sea water, *in* M.N. Hill, ed., The Sea, v. 2: New York, Wiley, p. 26-87.

Repeta, D.J., 1993, A high resolution historical record of Holocene anoxygenic primary production in the Black Sea: Geochimica et Cosmochimica Acta, v. 57, p. 4337-4342.

ROBL, T.L., RIMMER, S.M., AND BARRON, L.S., 1991, Organic petrography of Mississippian and Devonian shales in east-central Kentucky: Proceedings of the 1990 Eastern Oil Shale Symposium, Center for Applied Energy Research, Lexington, Kentucky, p. 173-178.

SCHIMMELMANN, A., AND KASTNER, M., 1993, Evolutionary changes over the last 1000 years of reduced sulfur phases and organic carbon in varved sediments of the Santa Barbara Basin, California: Geochim. Cosmochim. Acta, v. 57, p. 67-78.

SCHUTTER, S.R., 1983, Petrology, clay mineralogy, paleontology, and depositional environments of four Missourian (Upper Pennsylvanian) shales of Midcontinent and Illinois basins: University of Iowa, unpubl. Ph.D. Dissertation, 1208 p.

SCHUTTER, S.R., AND HECKEL, P.H., 1985, Missourian (Early Late Pennsylvanian) climate in Midcontinent North America: Internat. J. Coal Geol., v. 5, p. 111-140.

SCOTESE, C.R., 1994, Carboniferous paleocontinental reconstructions: U.S. Geol. Surv. Bull., v. 2110, p. 3-6.

SHIMMIELD, G.B., 1992, Can sediment geochemistry record changes in coastal upwelling palaeoproductivity? Evidence from northwest Africa and the Arabian Sea, *in* Summerhayes, C.P., Prell, W.L., and Emeis, K.C., eds., Upwelling Systems: Evolution Since the Early Miocene: Geological Society of London Special Publication 64, p. 29-46.

SMITH, R.L., 1992, Coastal upwelling in the modern ocean, *in* Summerhayes, C.P., Prell, W.L., and Emeis, K.C., eds., Upwelling Systems: Evolution Since the Early Miocene: Geological Society of London Special Publication 64, p. 9-28.

STEIN, R., 1991, Accumulation of Organic Carbon in Marine Sediments: Berlin, Springer, 217 pp.

TYSON, R.V., 1995, Sedimentary Organic Matter: Chapman & Hall, London, 615 pp.

VADSTEIN, O., JENSEN, A., OLSEN, Y., AND REINERTSEN, H., 1988, Growth and phosphorus status of limnetic phytoplankton and bacteria: Limnol. Oceanogr., v. 33, p. 489-503.

VEEVERS, J.J., AND POWELL, C.M., 1987, Late Paleozoic glacial episodes in Gondwanaland reflected in transgressive-regressive depositional sequences in Euramerica: Geological Society of America Bulletin, v. 98, p. 475-487.

WANLESS, H.R., AND WRIGHT, C.R., 1978, Paleoenvironmental maps of Pennsylvanian rocks, Illinois Basin and northern Midcontinent region: Geological Society of America Special Publication 23-MC, 30 p. & 165 figs.

WATNEY, W.L., 1980, Cyclic sedimentation of the Lansing-Kansas Groups in northwestern Kansas and southwestern Nebraska: Kansas Geological Survey Bulletin 220, 72 p.

WATNEY, W.L., FRENCH, J.A., AND FRANSEEN, E.K., 1989, Sequence stratigraphic interpretations and modeling of cyclothems in the Upper Pennsylvanian (Missourian) Lansing, and Kansas City groups in eastern Kansas: Kansas Geol. Soc., Lawrence, Kansas, 41st Annual Fieldtrip Guidebook, 211 pp.

WATNEY, W.L., FRENCH, J.A., DOVETON, J.H., YOULE, J.C., AND GUY, W.J., 1995, Cycle hierarchy and genetic stratigraphy of Middle and Upper Pennsylvanian strata in the upper Mid-continent, *in* Hyne, N.J., ed., Sequence Stratigraphy of the Mid-Continent: Tulsa, Oklahoma, Tulsa Geological Society Special Publication 4, p. 141-192.

WEAVER, C.E., 1989, Clays, Muds, and Shales: Amsterdam, Elsevier, 819 p.

WESTRICH, J.T., AND BERNER, R.A., 1984, The role of sedimentary organic matter in bacterial sulfate reduction: The G model tested: Limnol. Oceanogr., v. 29, p. 236-249.

WIGNALL, P.B., 1994, Black Shales: Oxford, Clarendon Press, 127 p.

Table 1.
Detrital-Element Concentrations
and Correlation Coefficients

	$\mu^\#$	$\sigma^\#$	SiO_2*	Al_2O_3*	Fe_2O_3*	K_2O*	MgO*	TiO_2*	Na_2O*
SiO_2*	56.7	±6.5	X	-.76	-.90	-.79	-.44	-.95	-.44
Al_2O_3*	23.9	±2.1	•	X	.61	.94	-.08	.77	.10
Fe_2O_3*	10.1	±3.2	•	•	X	.69	.20	.80	.28
K_2O*	5.8	±0.9	•	•	•	X	-.08	.78	.14
MgO*	2.3	±2.2	•		○		X	.43	.51
TiO_2*	1.1	±0.2	•	•	•	•	•	X	.41
Na_2O*	1.0	±0.4	•		•		•	•	X

\# Concentrations in weight percent.

* Concentrations recalculated to sum of detrital elements only.

Confidence limits: • = 1%, ○ = 5%.

TABLE 2.
MAJOR COMPONENT PROXY CORRELATIONS[#]

	TC	TS	P_2O_5	$Al_2O_3^*/SiO_2^*$
TC	X	.18	.11	.83
TS	-	X	-.02	.07
P_2O_5	-	-	X	-.24
$Al_2O_3^*/SiO_2^*$	●	-	○	X

[#] Correlation coefficients (*r*); n = 85.
Significance levels ($p(\alpha)$): ● = 0.1%, ○ = 5%.

FIGURE CAPTIONS

FIG. 1.--Location of the five study cores in eastern Kansas. Proximal (inner shelf) areas are to the north and distal (outer shelf) areas to the south. Missourian Stage outcrop and facies belts are redrawn from Heckel (1977).

FIG. 2.--Late Pennsylvanian paleogeography of midcontinent North America (from Heckel 1991, his figure 1). The study area is within the Kansas portion of the Midcontinent outcrop belt.

FIG. 3.--Missourian Stage stratigraphy of eastern Kansas. The three offshore black shale members examined in this study, the Hushpuckney, Stark, and Muncie Creek shales, are part of the Swope, Dennis, and Iola cyclothems, respectively. Sea-level curve redrawn and vertically rescaled from Boardman and Heckel (1989).

FIG. 4.--Time-space distribution of the eight study units and hierarchical sampling strategy. The eight study units represent three stratigraphic horizons (vertical axis) and five cores (horizontal axis). Symbols for individual study units (used for unit identification in subsequent figures) are shown in the lower panel. Hierarchical sampling entailed investigation of compositional variation in four "dimensions": (1) interformational variation (between black shale members), (2) geographic variation (between cores in the Hushpuckney and Stark shales), (3) intraformational variation (from the base to the top of each study unit), and (4) intracyclic variation (within dm-thick compositional cycles). X-radiograph GSD records (such as that shown for the Edmonds Stark) permitted optimization of sample locations for characterization of intraformational and intracyclic compositional variation.

FIG. 5.--Correlation and compositional analysis of the study units using X-radiography: (A) Stark Shale, (B) Hushpuckney and Muncie Creek shales, (C) legend for shaded fill patterns; compositional estimates are based on linear and multiple regression analysis (see text for discussion). In both A and B, the left column in each pair is a positive X-radiographic print in which lighter and darker hues represent lower- and higher-density areas of a core, respectively; lower density (relative to the shale matrix) is due mainly to increased organic carbon content, higher density to increased sulfide or phosphate content. Macroscopic dark layers and lenses are phosphate nodules; organic matter and sulfides tend to be finely disseminated through the shale matrix and not visible as discrete features. Note burrowing in the Hushpuckney Shale (>29 cm, Ermal and Mitchellson cores) and in the Muncie Creek Shale (>25 cm, Edmonds core). The right column in each pair gives the inferred geochemical composition of a study unit; relevant features include (1) column relief, which represents a continuous trace of gray-scale density (GSD) measurements along the central axis of each core X-radiograph (GSD units: 0 or white to left, 255 or black to right), and (2) shaded fill patterns, which represent the estimated organic carbon content of mm- to cm-thick layers in the study units based on TC-GSD correlations and which identify phosphate nodules based on visual inspection of the core X-radiographs (n.b., almost all P is present in macroscopic phosphate nodules; intervals containing nodules yielded >5 wt% P_2O_5, those lacking nodules <0.5 wt% P_2O_5). Scale to left of figure gives thickness above the base of the laminated black-shale facies; >80% of the thickness of laminated black shale facies in each study unit is shown (range of thicknesses is 36-55 cm). Correlations between study cores are represented as dashed lines; dm-thick compositional couplets are numbered for reference.

FIG. 6.--Dendrogram of major- and trace-element relations based on R-mode cluster analysis; the distance metric was the Pearson correlation coefficient (*r*) and the linkage protocol was the weighted pair-group centroid method. Phenon lines were chosen to (1) coincide with similarity coefficient ranges containing few linkages and (2) yield a small number of interpretable elemental clusters. The results shown are based on all samples from the eight study units ($n = 85$); similar results were obtained for individual shale members.

FIG. 7.--Detrital-element covariation patterns. Both K_2O* (A) and TiO_2* (B) exhibit strong positive covariance with Al_2O_3*/SiO_2* ($r^2 = 0.80$ and 0.86, respectively; $p(\alpha) < .001$; $n = 85$, i.e., all samples from the eight study units; asterisks indicate that elemental concentrations are normalized to a volatile-free basis). Strong covariance is indicative of mixing of two dominant clay minerals, i.e., smectite and illite. (C) Section-mean values for TiO_2* vs. Al_2O_3*/SiO_2*: means μ are given as symbols, ranges of the standard error of the mean $s/\sqrt{n}$ as open rectangles, and ranges of the standard deviation *s* as crosses. Section-mean values exhibit a strong geographic dependency, in which northern locales (Edmonds) exhibit higher means as well as greater variation in TiO_2* and Al_2O_3*/SiO_2* relative to midshelf (Ermal, Womelsdorf, and Mitchellson) or southern locales (Heilman). Symbols as in Figure 4.

FIG. 8.--Variation in organic maceral frequency ratios (A) and organic carbon C-isotopic compositions (B) as a function of total organic carbon concentration (n.b., given as volume percent in A and as weight percent in B). Note (1) positive covariation of inertinite/vitrinite ratios with TOC for all three shales at the Edmonds locale (ED; dashed fields) in A, and (2) positive covariation of organic carbon $\delta^{13}C$ values with TOC for the Hushpuckney and Muncie Creek shales in B. Symbols as in Figure 4.

FIG. 9.--(A) Ichnological and geochemical indicators of degree-of-anoxia (DOA). Oxygen-related zones were established on ichnological criteria: the anoxic zone (ca. 0-0.2 ml O_2 l^{-1} H_2O) corresponds to laminated sediments and the suboxic zone (ca. 0.2-0.5 ml O_2 l^{-1} H_2O) to weakly bioturbated sediments. Values of geochemical proxies of DOA represent estimates for the lower and upper boundaries of the anoxic zone. (B) Inferred spatio-temporal relations between bottomwater O_2 levels and P_2O_5 concentrations in the study units. Because all DOA proxies suggest decreasing O_2 levels northward within the Hushpuckney and Stark shales, divergent regional trends in P_2O_5 concentrations imply differences in P cycling mechanisms between black shale members.

FIG. 10.--(A) Calculated volumetric fractions of major components of the Hushpuckney, Stark, and Muncie Creek shales. (B) Illite/smectite (I/S) and vitrinite/inertinite (Vt/In) ratios for the three study shales. Note the strong north-south gradients in component volumes (A) and clay mineral and organic maceral ratios (B) in both the Hushpuckney and Stark shales.

FIG. 11.--Relationship of organic carbon to clay mineral, Fe-sulfide, and phosphate abundances, as proxied by TC vs. Al_2O_3*/SiO_2* (A), TS (B), and P_2O_5 (C), respectively (*n* = 85, i.e., all samples from the eight study units). TC exhibits strong positive (non-linear) covariation with Al_2O_3*/SiO_2* ($r^2 = 0.81$; $p(\alpha) < .001$); weak positive covariation with TS ($r^2 = 0.15$; $p(\alpha) > .05$; n.b., "normal marine" line from Berner and Raiswell 1983); and a complex relationship with P_2O_5, in which samples with low (<15 wt%) or high (>32 wt%) TC concentrations yield uniformly low P_2O_5 values and those with intermediate TC concentrations (15-32 wt%) yield variably low to high P_2O_5 values (n.b., weighted running averages shown as solid line for Hushpuckney Shale and dashed line for Stark Shale). Symbols as in Figure 4.

FIG. 12.--Relationship of clay minerals to phosphate abundance, as proxied by Al_2O_3*/SiO_2* vs. P_2O_5. Dashed line separates low Al_2O_3*/SiO_2* field characterized by variable P_2O_5 values from high Al_2O_3*/SiO_2* field characterized by uniformly low P_2O_5 values. Symbols as in Figure 4.

FIG. 13.--Molar C/P ratios for the Hushpuckney, Stark, and Muncie Creek shales (*n* = 80; n.b., data bins plotted on a logarithmic scale). Three frequency modes exist, i.e., one (C/P_{mol} = 100-150) close to the Redfield ratio for marine phytoplankton ($C/P_{mol} \approx 106:1$), one (C/P_{mol} = 600-1500) close to values associated with terrigenous organic matter, and one (C/P_{mol} = 15-40) associated with macroscopic phosphate nodules and reflecting strong P enrichment of the sediment. All three modes are present in the Hushpuckney and Stark shales; insufficient data preclude recognition of independent modes in the Muncie Creek Shale.

FIG. 14.--Interpretative north-south cross-section of environmental conditions on the Eastern Midcontinent Shelf during deposition of the study shales. Regional trends in the concentrations of organic carbon, Fe-sulfide, phosphate, and redox-sensitive trace elements (e.g., Mo, U_{exc}, and V) reflect lateral redox gradients, which were due to freshwater runoff from the north, producing a strong proximal halocline a weak distal thermocline (cf. Heckel 1991). Systematic differences in degree-of-anoxia proxies between study formations imply secular variation in redox conditions between cyclothems at maximum transgression: the Muncie Creek environment was the least oxygen depleted (A) and the Stark environment the most strongly anoxic (B). Low but fluctuating O_2 levels (diagonally lined fields) promoted phosphate nodule formation in proximal parts of the Hushpuckney environment (C); see text for discussion. Geographic header at top; horizontal scale is approximate.

FIG. 15.--Interpretative view of authigenic phosphate formation. At uniformly low dissolved O_2 levels (e.g., Stark environment), remineralization of organic carbon releases PO_4^{3-} into porewaters and reduction of Fe prevents adsorption of PO_4^{3-} onto Fe-oxyhydroxides, allowing PO_4^{3-} to escape upward. At low but fluctuating O_2 levels (e.g., Hushpuckney environment), PO_4^{3-} is adsorbed onto solid Fe-oxyhydroxide compounds forming along the redox interface, allowing sufficient time for downward diffusion of Ca^{2+} and F^- and growth of phosphate nodules. At higher (suboxic) O_2 levels (e.g., Muncie Creek environment), oxidation of labile organic matter in the near-surface environment allows PO_4^{3-} to diffuse upward without being retained by Fe-oxyhydroxides (cf. Jarvis et al. 1994).

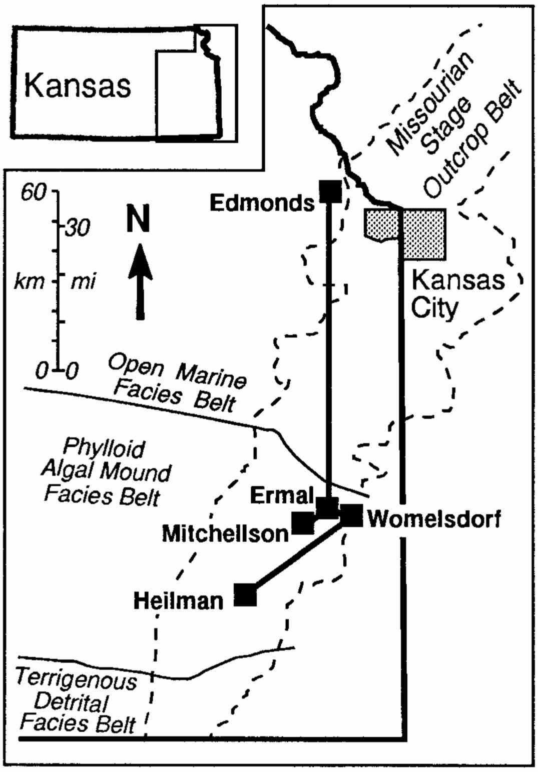
Kansas
Missourian Stage Outcrop Belt
60
30
km
mi
0
0
N
Edmonds
Kansas City
Open Marine Facies Belt
Phylloid Algal Mound Facies Belt
Ermal
Womelsdorf
Mitchellson
Heilman
Terrigenous Detrital Facies Belt

Figure 1

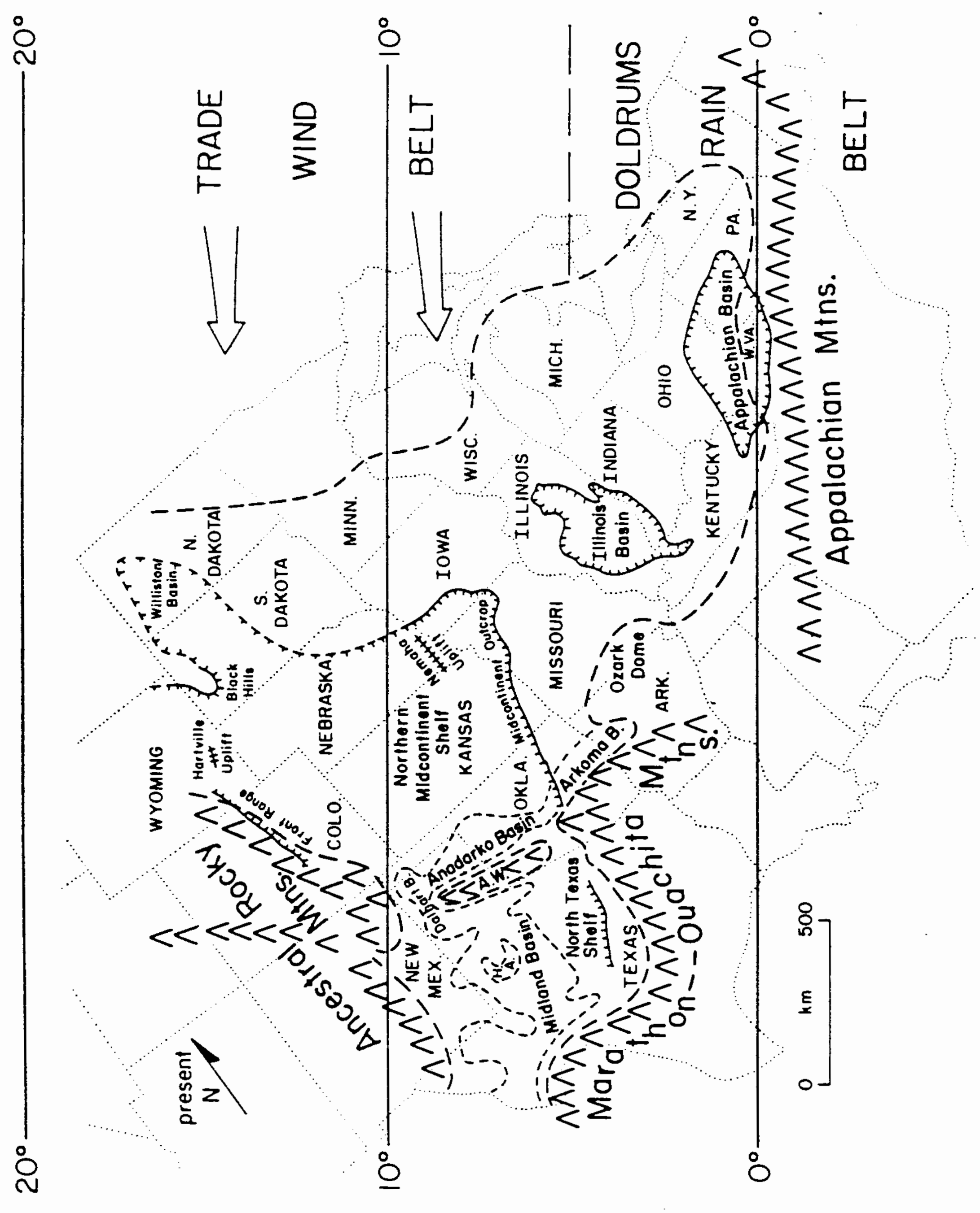
20°
20°
10°
10°
0°
0°
TRADE
WIND
BELT
DOLDRUMS
RAIN
BELT
present N
WYOMING
Hartville Uplift
Black Hills
Williston Basin
N. DAKOTA
S. DAKOTA
MINN.
NEBRASKA
COLO.
Front Range
Ancestral Rocky Mtns.
Northern Midcontinent Shelf
KANSAS
IOWA
Nemaha Uplift
Midcontinent Outcrop
MISSOURI
WISC.
ILLINOIS
Illinois Basin
INDIANA
MICH.
OHIO
KENTUCKY
N.Y.
PA.
Appalachian Basin
W. VA.
Appalachian Mtns.
OKLA.
Arkoma B.
Ozark Dome
ARK.
Ouachita Mtns.
Anadarko Basin
A.W.
Dalhart B.
NEW MEX.
Midland Basin
North Texas Shelf
TEXAS
Marathon
0
km
500

Figure 2

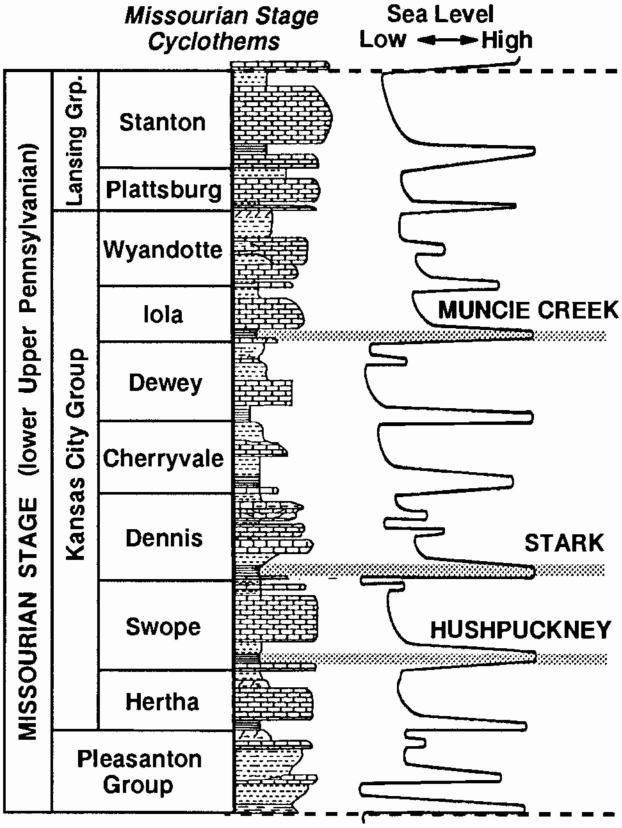
Missourian Stage Cyclothems
Sea Level
Low ◄—► High
MISSOURIAN STAGE (lower Upper Pennsylvanian)
Lansing Grp.
Kansas City Group
Stanton
Plattsburg
Wyandotte
Iola
Dewey
Cherryvale
Dennis
Swope
Hertha
Pleasanton Group
MUNCIE CREEK
STARK
HUSHPUCKNEY

Figure 3

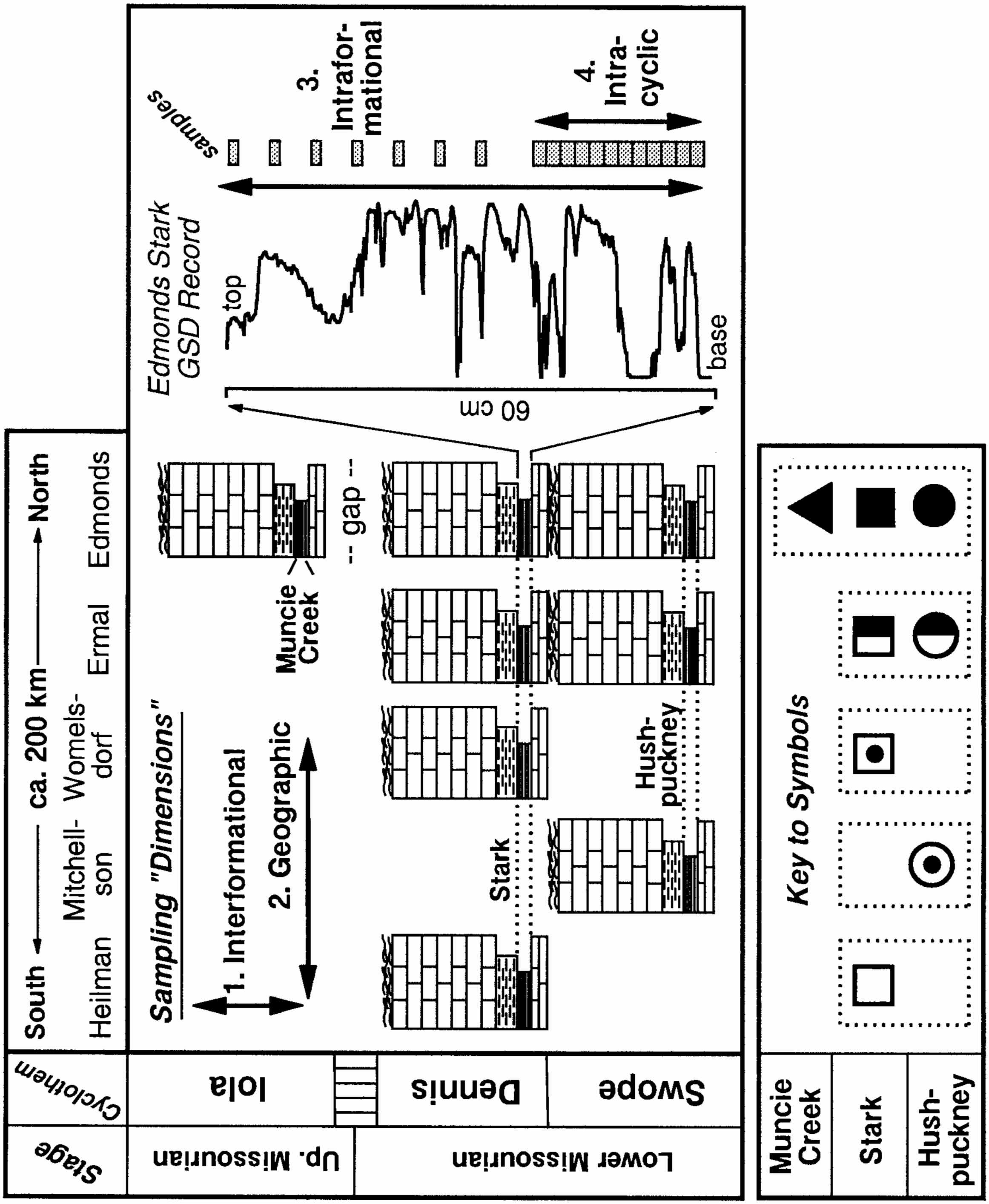
Stage
Cyclothem
Up. Missourian
Lower Missourian
Iola
Dennis
Swope
South
ca. 200 km
North
Heilman
Mitchell-son
Womels-dorf
Ermal
Edmonds
Sampling "Dimensions"
1. Interformational
2. Geographic
Stark
Muncie Creek
Hush-puckney
-- gap --
60 cm
Edmonds Stark GSD Record
top
base
samples
3. Intrafor-mational
4. Intra-cyclic
Key to Symbols
Muncie Creek
Stark
Hush-puckney

Figure 4

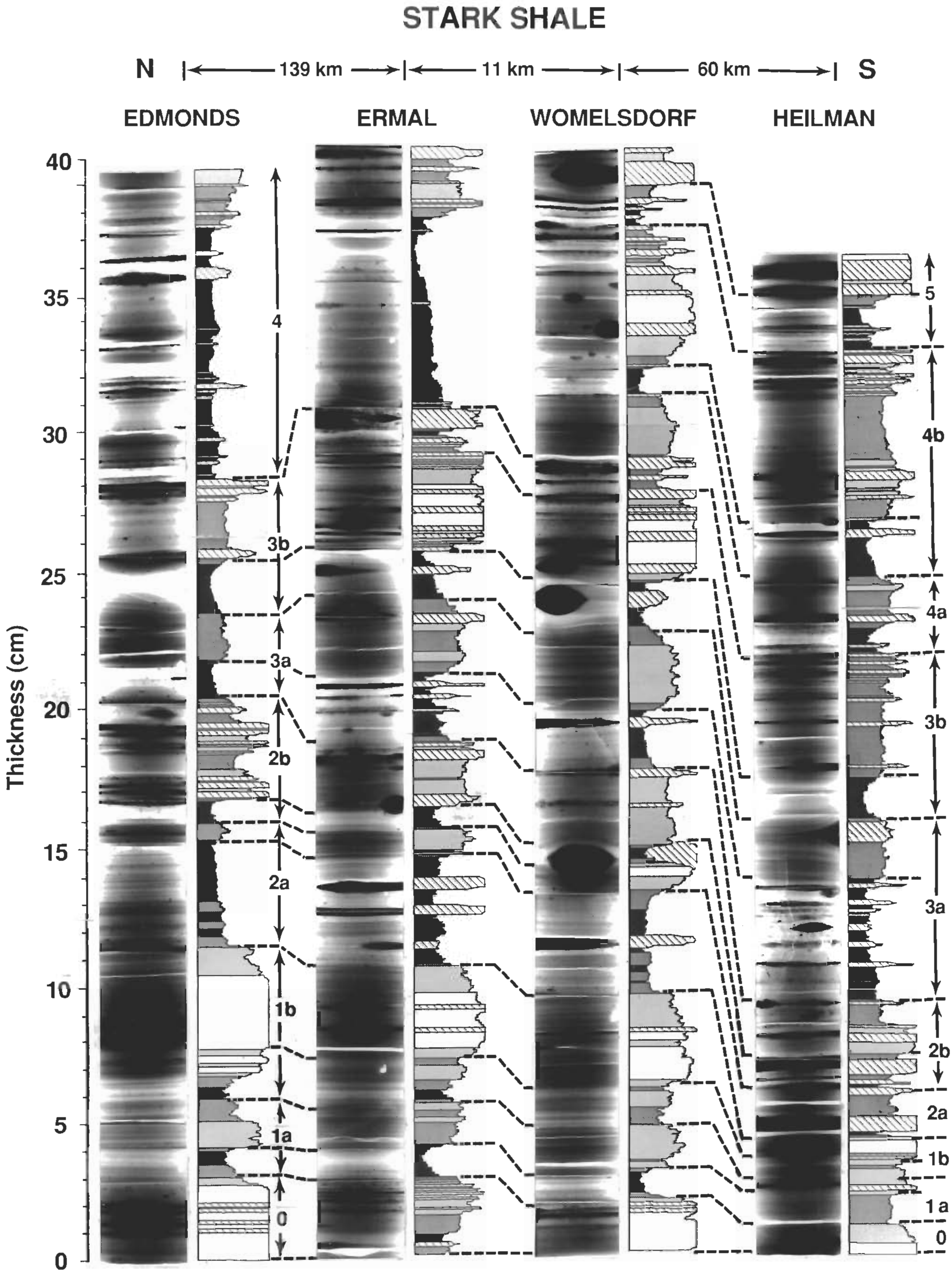
STARK SHALE
N
139 km
11 km
60 km
S
EDMONDS
ERMAL
WOMELSDORF
HEILMAN
Thickness (cm)
0
5
10
15
20
25
30
35
40
4
3b
3a
2b
2a
1b
1a
0
5
4b
4a
3b
3a
2b
2a
1b
1 a
0

Figure 5A

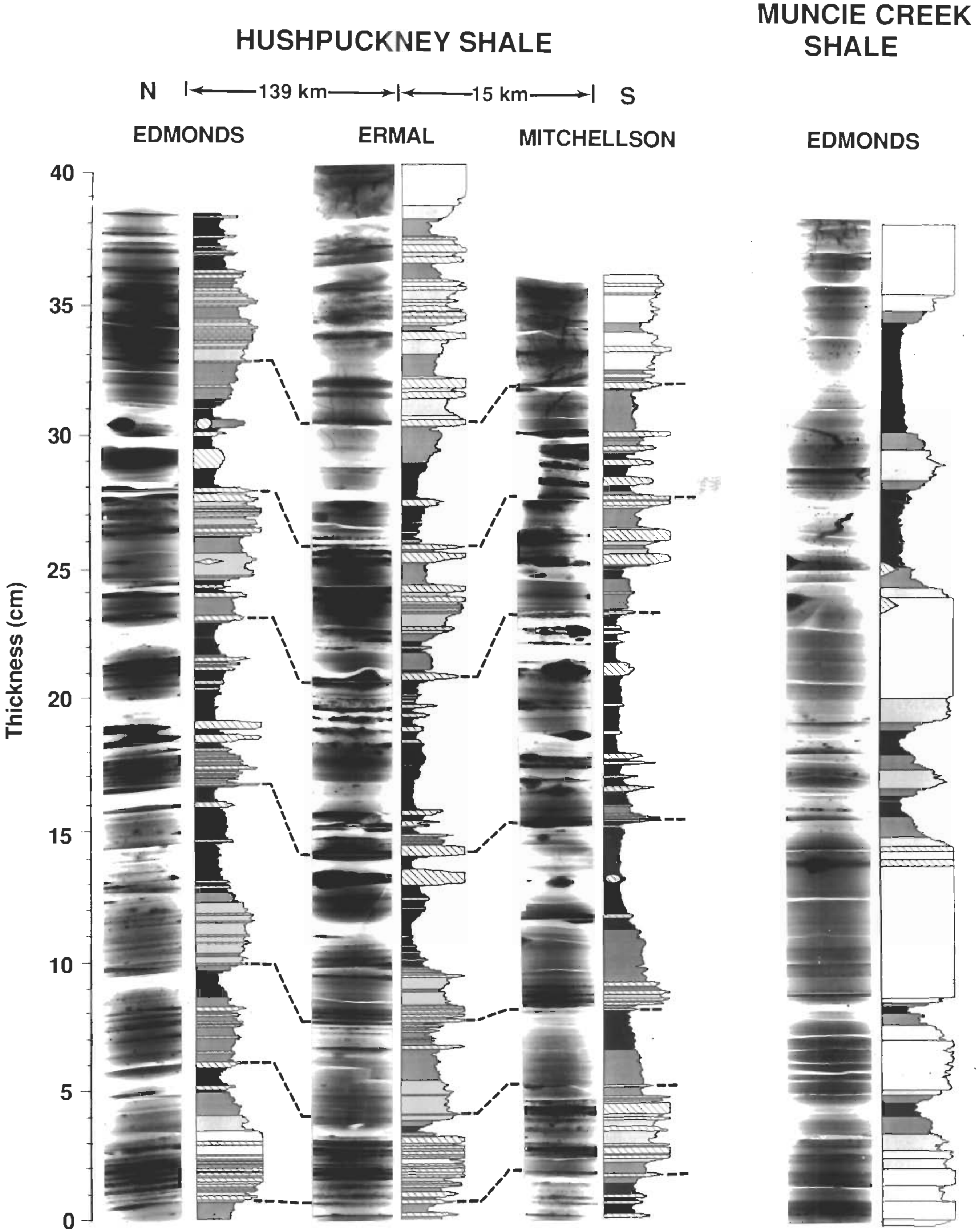

HUSHPUCKNEY SHALE

MUNCIE CREEK SHALE

Figure 5B

	STARK					**HUSHPUCKNEY**			**MUNCIE CREEK**
	TC				TS	TC		P_2O_5	TC
	Edmonds	Ermal	Womelsdorf	Heilman		Edmonds	Ermal	Mitchellson	Edmonds
■	>35	>20	>30	>20	<1.6	>25	>25	<2	>30
▩	25-35	15-20	20-30	15-20	1.6-2.0	20-25	20-25	2-6	20-30
▒	15-25	10-15	10-20	10-15	2.0-2.4	15-20	15-20	6-10	10-20
□	<15	<10	<10	<10	>2.4	<15	<15	>10	<10

▨ Phosphate nodules (all sections)

Note: all values in weight percent.

Figure 5C

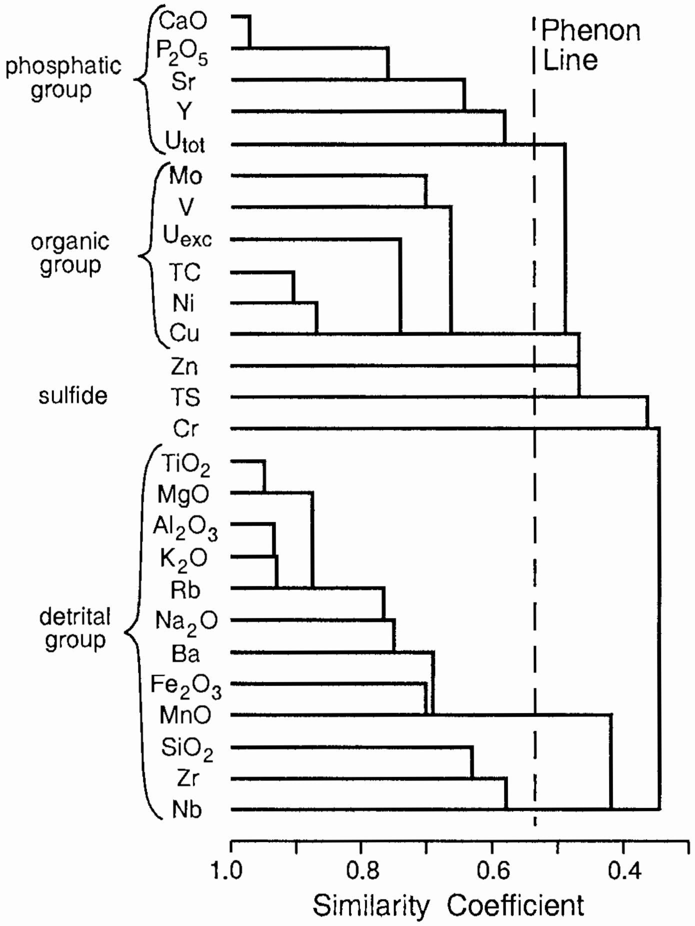
phosphatic group
CaO
P_2O_5
Sr
Y
U_{tot}
organic group
Mo
V
U_{exc}
TC
Ni
Cu
sulfide
Zn
TS
Cr
detrital group
TiO_2
MgO
Al_2O_3
K_2O
Rb
Na_2O
Ba
Fe_2O_3
MnO
SiO_2
Zr
Nb
Phenon Line
1.0
0.8
0.6
0.4
Similarity Coefficient

Figure 6

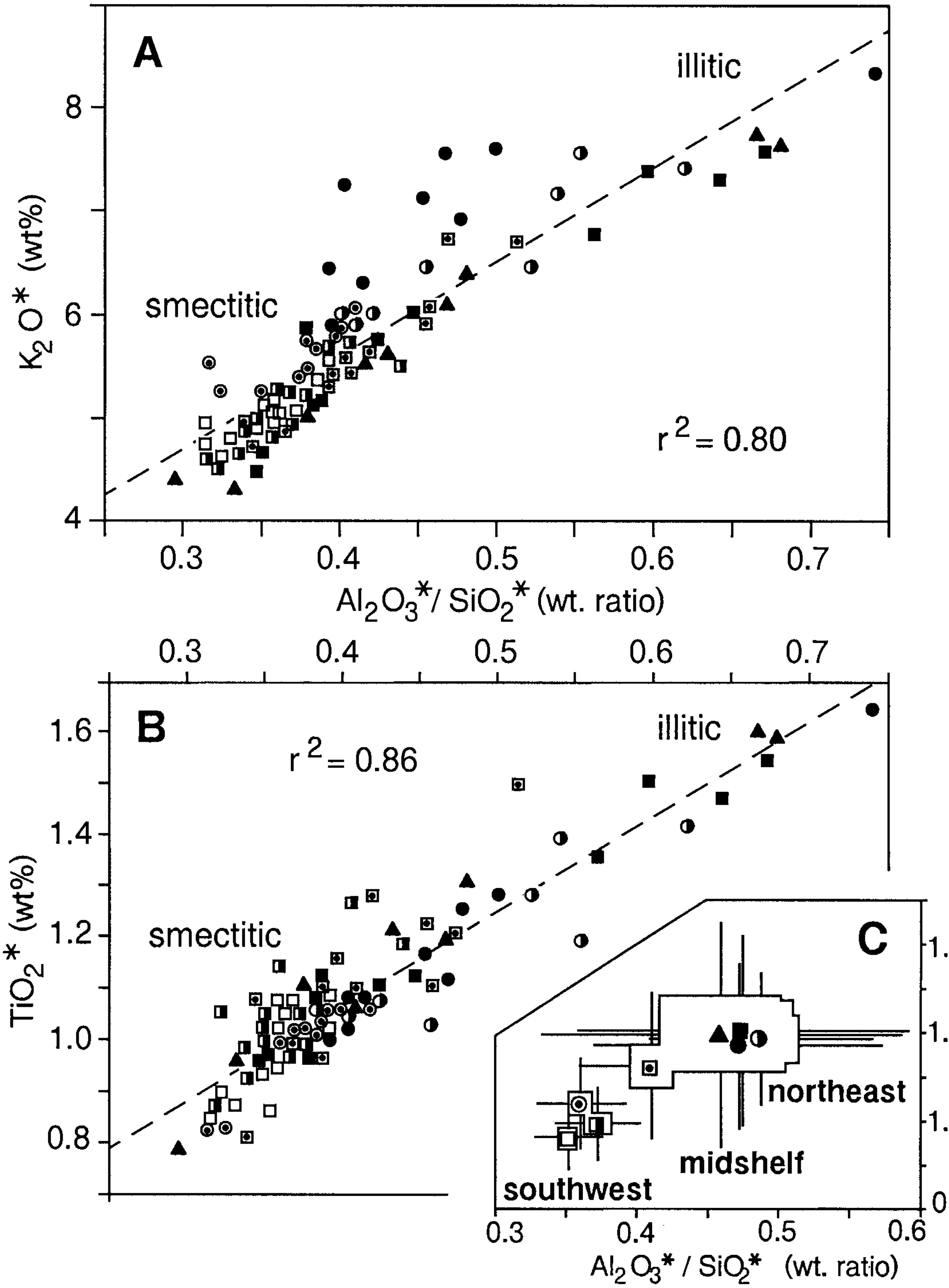
A
illitic
smectitic
r² = 0.80
K_2O^* (wt%)
8
6
4
0.3
0.4
0.5
0.6
0.7
$Al_2O_3^*/SiO_2^*$ (wt. ratio)
B
r² = 0.86
illitic
smectitic
TiO_2^* (wt%)
1.6
1.4
1.2
1.0
0.8
C
northeast
midshelf
southwest
1.4
1.2
1.0
0.8
TiO_2^* (wt%)
$Al_2O_3^*/SiO_2^*$ (wt. ratio)

Figure 7

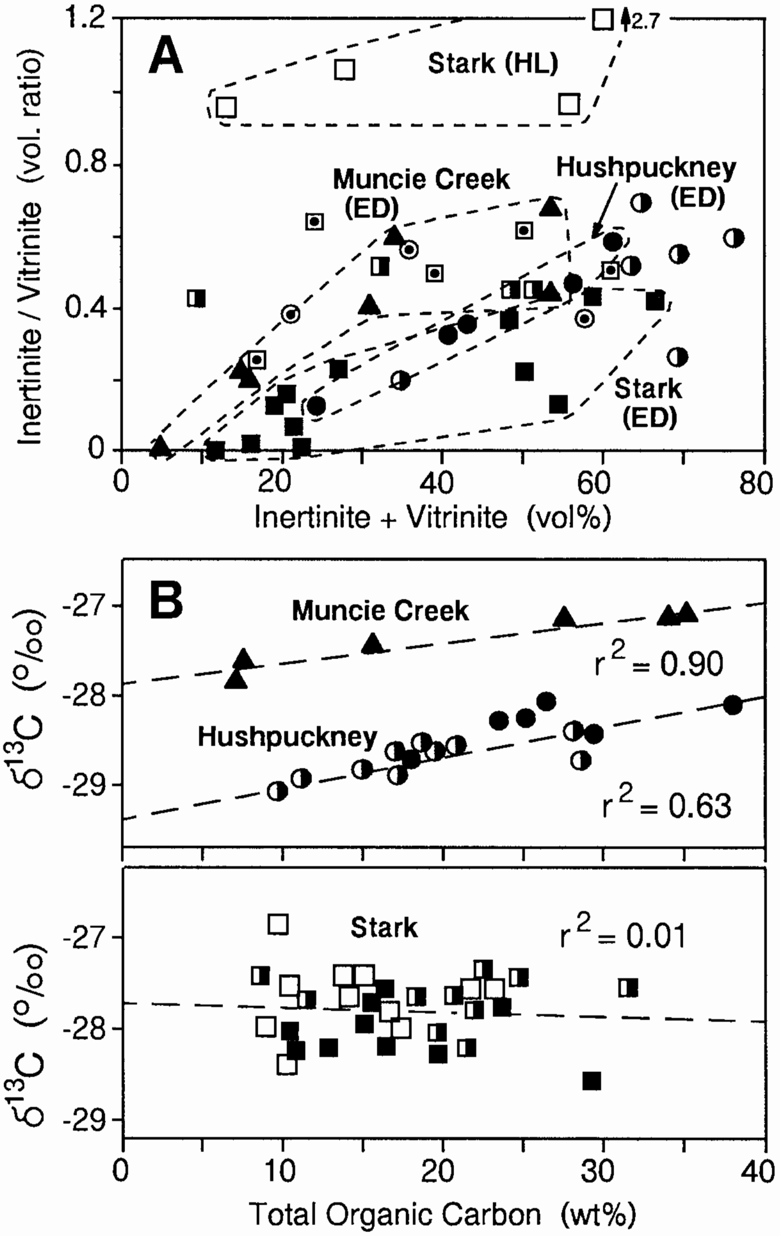
A
Stark (HL)
2.7
Muncie Creek (ED)
Hushpuckney (ED)
Stark (ED)
Inertinite / Vitrinite (vol. ratio)
1.2
0.8
0.4
0
0
20
40
60
80
Inertinite + Vitrinite (vol%)
B
Muncie Creek
$r^2 = 0.90$
Hushpuckney
$r^2 = 0.63$
$\delta^{13}C$ (‰)
-27
-28
-29
Stark
$r^2 = 0.01$
$\delta^{13}C$ (‰)
-27
-28
-29
0
10
20
30
40
Total Organic Carbon (wt%)

Figure 8

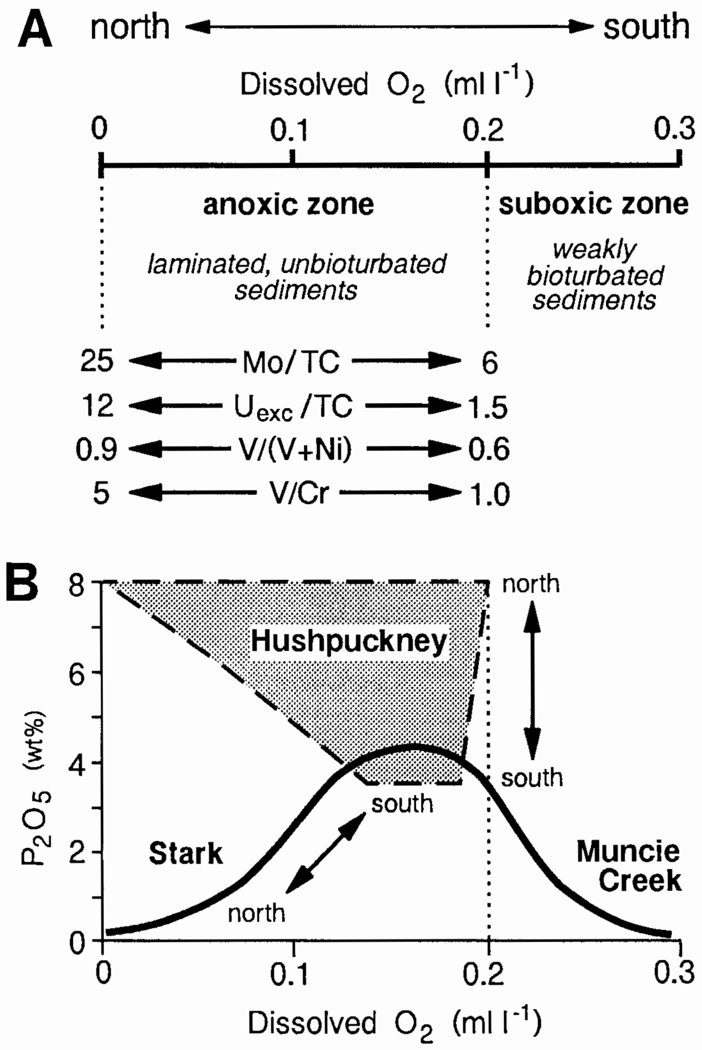
A
north
south
Dissolved O2 (ml l-1)
0
0.1
0.2
0.3
anoxic zone
suboxic zone
laminated, unbioturbated sediments
weakly bioturbated sediments
25
Mo/TC
6
12
Uexc /TC
1.5
0.9
V/(V+Ni)
0.6
5
V/Cr
1.0
B
8
6
4
2
0
P2O5 (wt%)
Hushpuckney
north
south
south
north
Stark
Muncie Creek
0
0.1
0.2
0.3
Dissolved O2 (ml l-1)

Figure 9

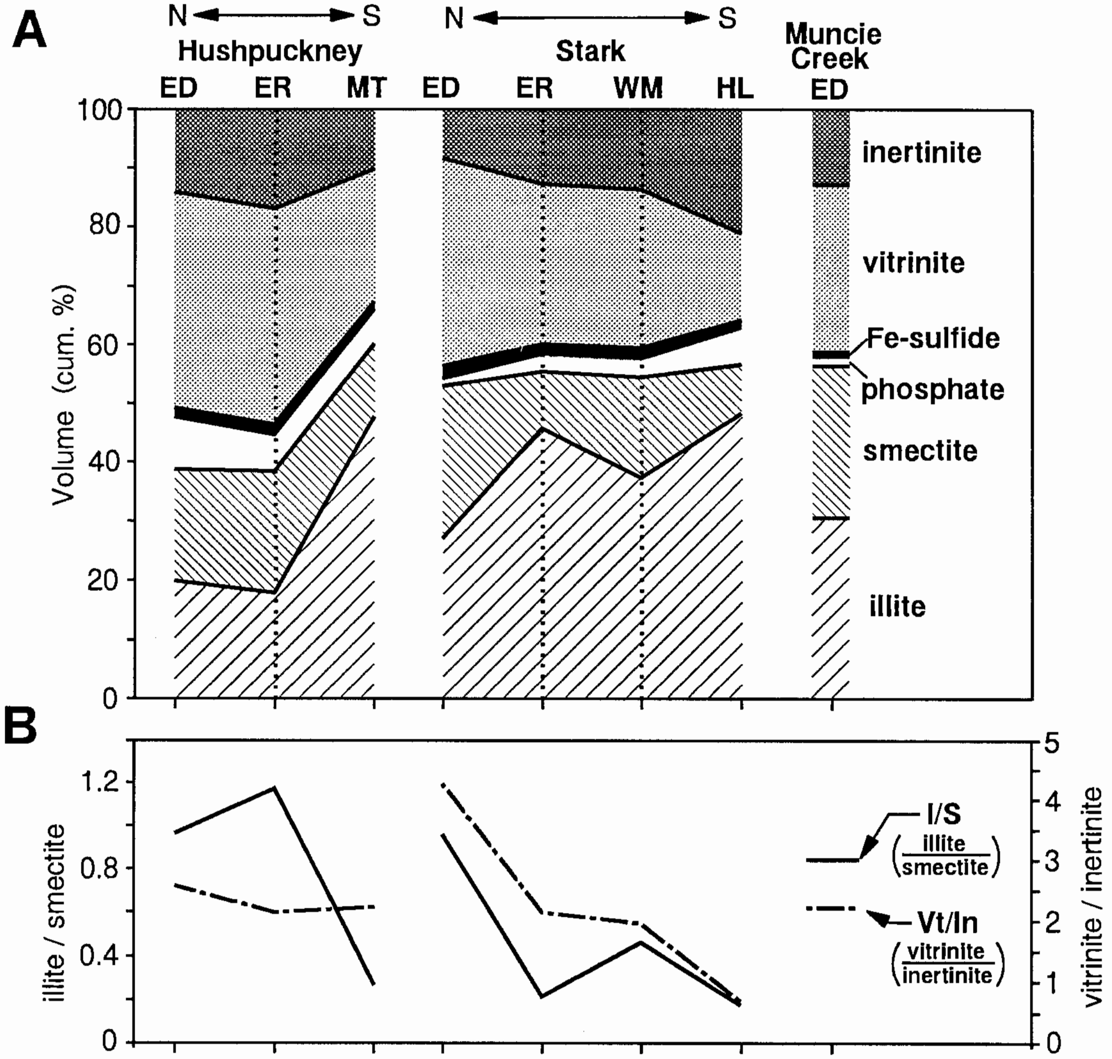
A
N ← → S
Hushpuckney
ED
ER
MT
N ← → S
Stark
ED
ER
WM
HL
Muncie Creek
ED
100
80
60
40
20
0
Volume (cum. %)
inertinite
vitrinite
Fe-sulfide
phosphate
smectite
illite
B
1.2
0.8
0.4
0
illite / smectite
5
4
3
2
1
0
vitrinite / inertinite
I/S
(illite / smectite)
Vt/In
(vitrinite / inertinite)

Figure 10

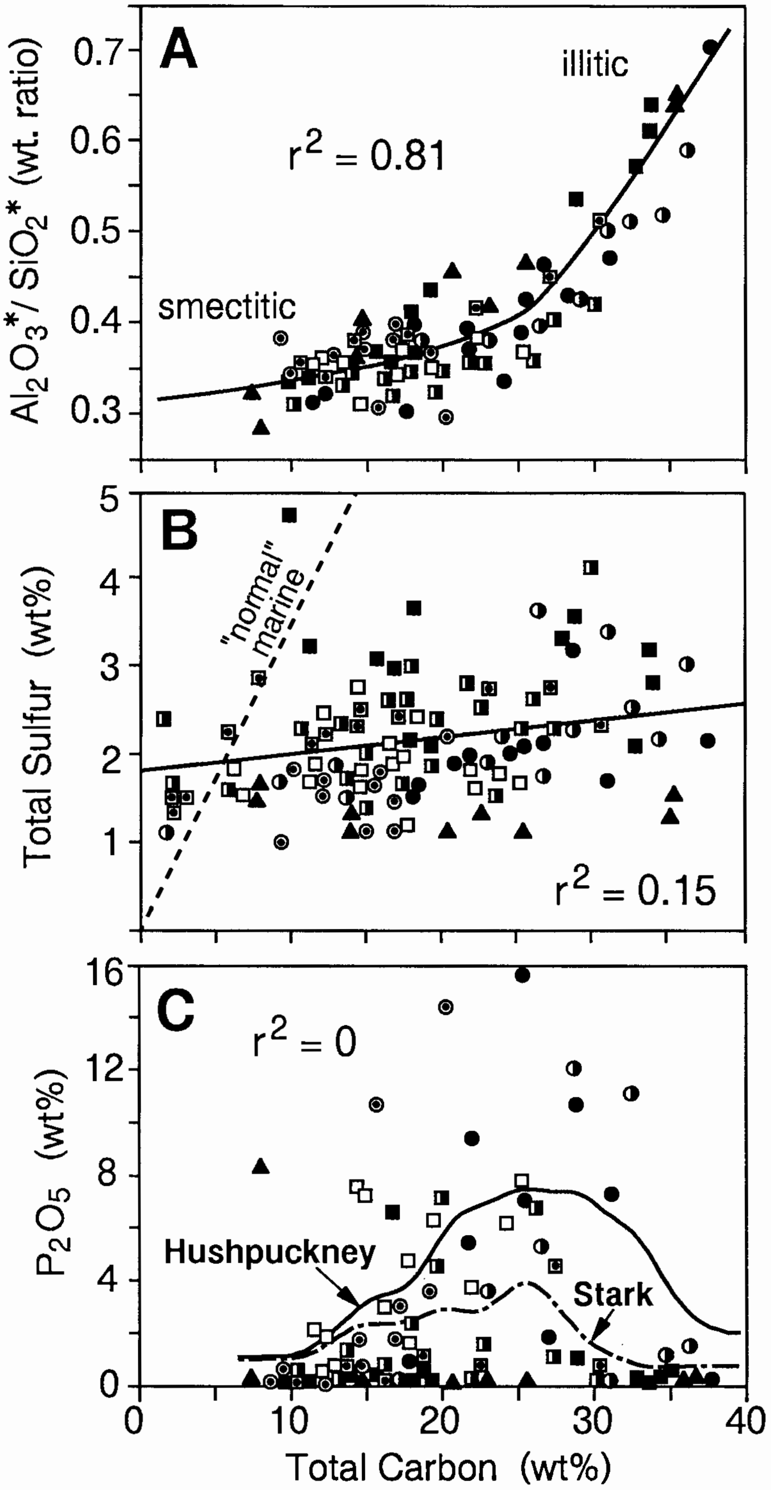
A
$Al_2O_3^*/SiO_2^*$ (wt. ratio)
0.3
0.4
0.5
0.6
0.7
illitic
$r^2 = 0.81$
smectitic
B
Total Sulfur (wt%)
1
2
3
4
5
"normal" marine
$r^2 = 0.15$
C
P_2O_5 (wt%)
0
4
8
12
16
$r^2 = 0$
Hushpuckney
Stark
0
10
20
30
40
Total Carbon (wt%)

Figure 11

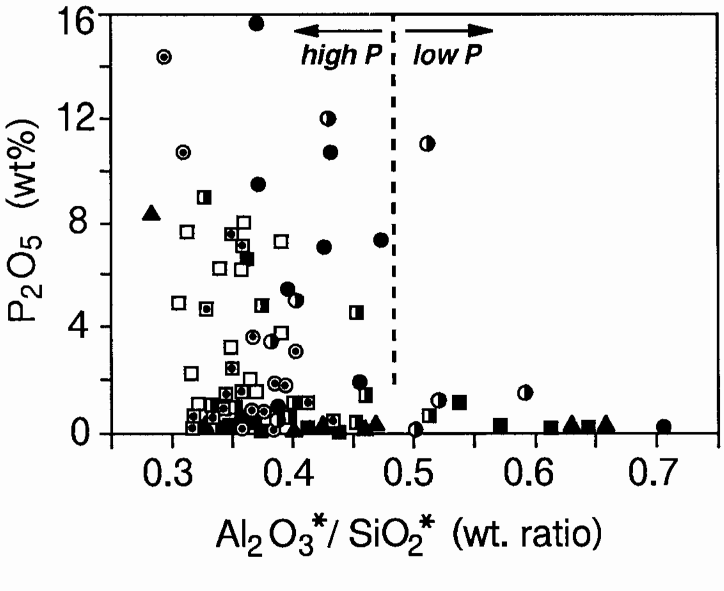

Figure 12

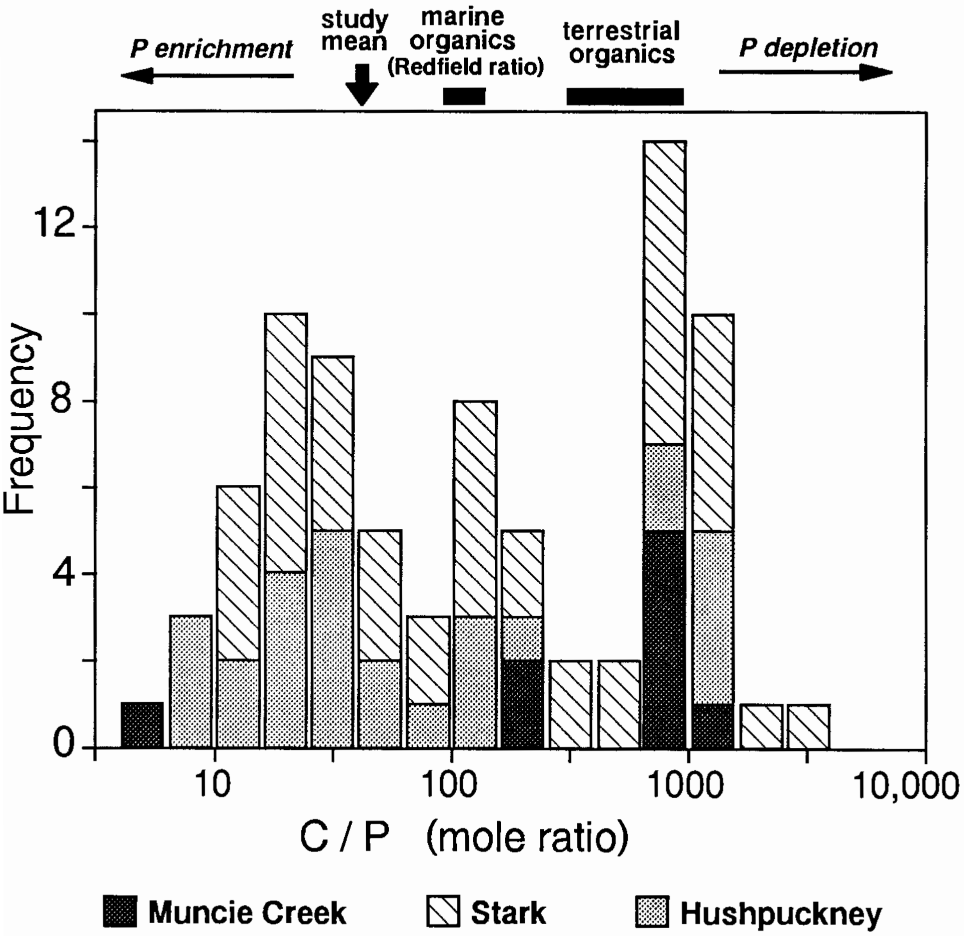
P enrichment
study mean
marine organics (Redfield ratio)
terrestrial organics
P depletion
Frequency
0
4
8
12
10
100
1000
10,000
C / P (mole ratio)
Muncie Creek
Stark
Hushpuckney

Figure 13

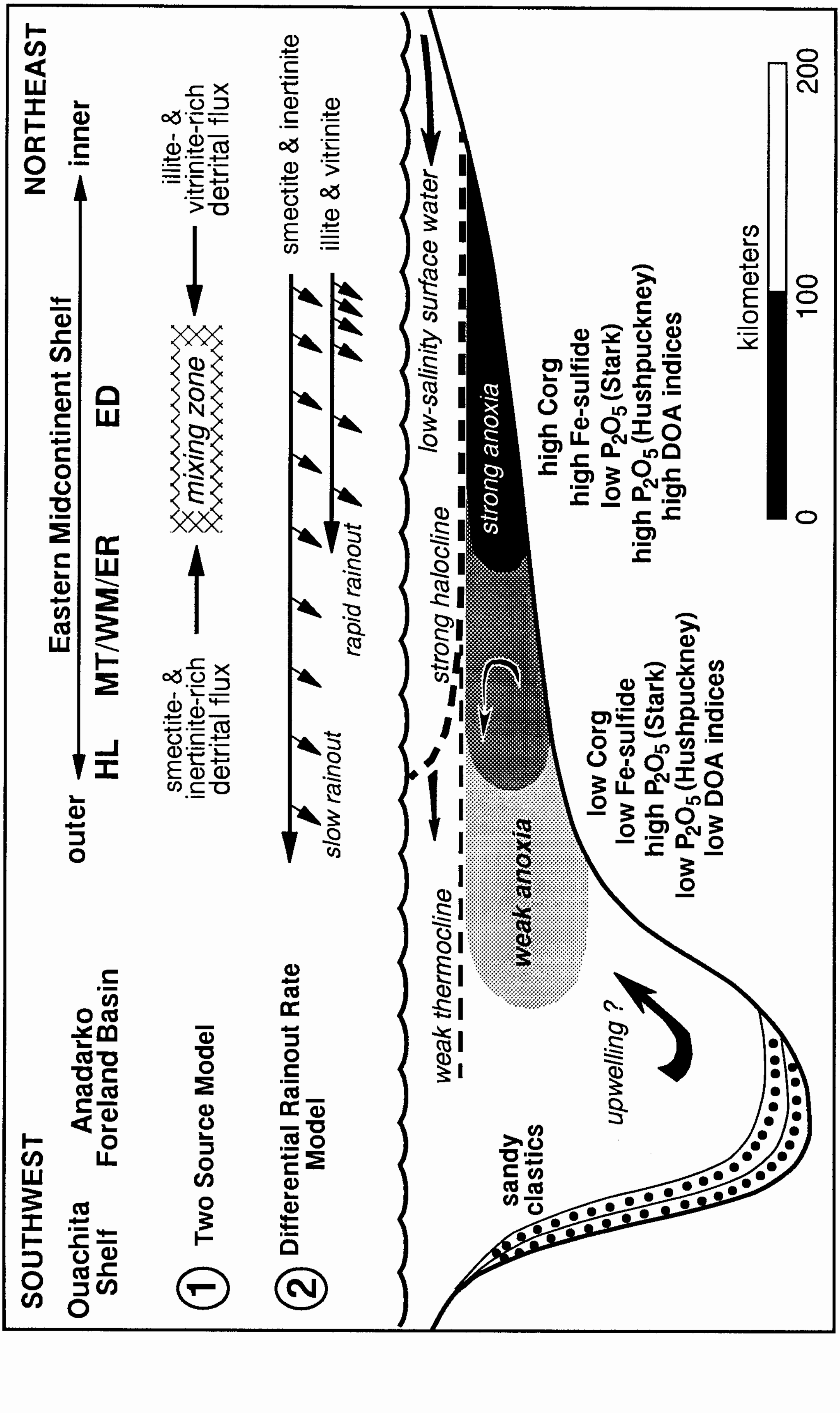
SOUTHWEST
NORTHEAST
Ouachita Shelf
Anadarko Foreland Basin
Eastern Midcontinent Shelf
outer
inner
HL
MT/WM/ER
ED
① Two Source Model
smectite- & inertinite-rich detrital flux
mixing zone
illite- & vitrinite-rich detrital flux
② Differential Rainout Rate Model
slow rainout
rapid rainout
smectite & inertinite
illite & vitrinite
weak thermocline
strong halocline
low-salinity surface water
sandy clastics
upwelling ?
weak anoxia
strong anoxia
low Corg
low Fe-sulfide
high P_2O_5 (Stark)
low P_2O_5 (Hushpuckney)
low DOA indices
high Corg
high Fe-sulfide
low P_2O_5 (Stark)
high P_2O_5 (Hushpuckney)
high DOA indices
kilometers
0
100
200

Figure 14

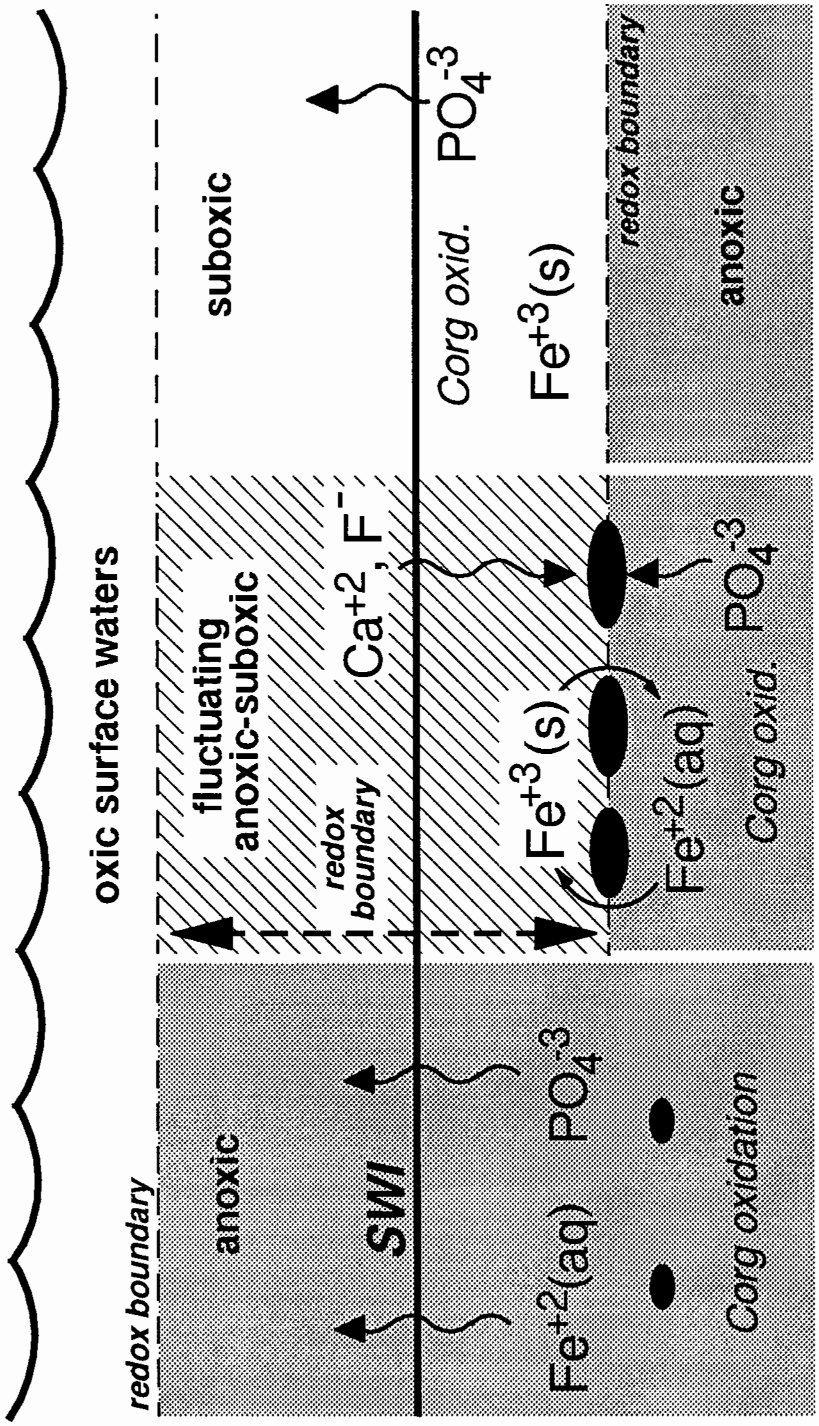
STARK
HUSHPUCKNEY
MUNCIE CREEK
oxic surface waters
redox boundary
anoxic
SWI
$Fe^{+2}(aq)$
PO_4^{-3}
Corg oxidation
fluctuating anoxic-suboxic
redox boundary
Ca^{+2}, F^-
$Fe^{+3}(s)$
$Fe^{+2}(aq)$
Corg oxid.
PO_4^{-3}
suboxic
Corg oxid.
$Fe^{+3}(s)$
PO_4^{-3}
redox boundary
anoxic

Figure 15